INVESTIGATING SEDIMENT SOURCE TO SINK PROCESSES IN A POST-OROGENIC LANDSCAPE

A Thesis
Presented to
The Academic Faculty

by

Tina L. Marstellar

In Partial Fulfillment
of the Requirements for the Degree
Master of Science in the
School of Earth and Atmospheric Science

Georgia Institute of Technology
May 2012

INVESTIGATING SEDIMENT SOURCE TO SINK PROCESSES IN A POST-OROGENIC LANDSCAPE

Approved by:

Dr. Kurt L. Frankel, Advisor
School of Earth and Atmospheric Science
Georgia Institute of Technology

Dr. Patrick Belmont
College of Natural Resources
Watershed Sciences Department
Utah State University

Dr. Ellery Ingall
School of Earth and Atmospheric Sciences
Georgia Institute of Technology

Dr. Andrew Newman
School of Earth and Atmospheric Sciences
Georgia Institute of Technology

Date Approved: January 11, 2012

This paper is dedicated to the memory of Kurt Lang Frankel, a treasured advisor, teacher, mentor, and friend.

ACKNOWLEDGEMENTS

First and foremost, I wish to thank my advisor, Dr. Kurt Frankel, for his extreme patience and guidance. Kurt provided many laughs – mostly at my expense – but made the experience of research enormously fun with his humor. As the first female student of Kurt's, I had the joy of spending several hours with many great guys, and we eventually added another female to the group. I am grateful for the laughs provided by the Frankel research group (Kurt, Jeff, Andy, Zach, Chris, and Chelsea) and the ability to work with all of these intelligent and entertaining people.

I spent many hours kicking myself for deciding to take on the endeavor of writing a thesis - even more so after Kurt's passing in July of 2011. I was fortunate to be adopted by Dr. Patrick Belmont at Utah State University. Patrick filled a large void and I am forever indebted to him for his assistance in bringing this thesis to completion. Patrick holds the same wonderful characteristics as Kurt, patience and tolerance, which are required when taking me on as a student. His encouragement and persistence kept me from giving up on what seemed to be in insurmountable task.

I had several dedicated field assistants. Molly Lindle-Gowen traveled to north Georgia and North Carolina on short notice and provided many laughs along the way. Kelli Hornberger suffered great pain, and still has the scars to show it, after one difficult climb through thorns and over moss covered bedrock. Rebecca Westby listened to me whine over blistered and bleeding feet for at least three miles of hiking with wet shoes. She had a smile on her face the entire time – probably because she wore sensible shoes. And lastly, Jeff Hoeft actually paid money to join me in the field. He didn't give up the

money voluntarily, but none the less, he was cash-out-of-pocket after an adventure to the field with me and Kurt. I wish to thank them all for their encouragement and laughter along the way. I would also like to thank my thesis reading committee of Andrew Newman and Ellery Ingall. They provided thoughtful reviews to improve this manuscript.

I wish to thank my amazing daughters, Melanie and McKenzie. They suffered through some very stressful times while I was completing this thesis and they helped to remind me what is most important in life. They gave me many reasons to smile when I often felt like crying. There is nothing that a hug from them can't cure.

This research was funded by ACS Petroleum Research Fund grant number 48871-DNI8, National Science Foundation grant number EAR-0929960, Sigma Xi, and Geological Society of America, Southeastern section.

TABLE OF CONTENTS

LIST OF TABLES

LIST OF FIGURES

LIST OF ABBREVIATIONS

Be	beryllium
AMS	accelerator mass spectrometry
DEM	digital elevation model
H_20	purified water
HCl	hydrochloric acid
HI	hypsometric integral
HF	hydrofluoric acid
HNO_3	nitric acid
LLNL-CAMS	Lawrence Livermore National Lab – Center for Accelerator Mass Spectrometry
NED	national elevation dataset
SLHL	sea-level, high-latitude
TCN	terrestrial cosmogenic nuclide
V/A	volume to area

SUMMARY

In order to understand the life cycle of a mountain range, it is crucial to identify and quantify the processes that influence the rate of denudation, sediment flux through the landscape, and the resulting changes in relief over long time scales in tectonically-inactive regions. Geologic history and the quartz-rich lithologies make the southern Appalachian Mountains an ideal location for terrestrial cosmogenic nuclide (TCN) measurements aimed at studying erosion and denudation processes in an evolving post-orogenic landscape. We used in situ-produced TCN measurements of Beryllium-10 (^{10}Be) to determine the denudation rate in ten catchments along the southern Appalachians. The locations selected are all within the east-draining Blue Ridge escarpment in North Carolina and Georgia. In five of the ten catchments we sampled two grain sizes, gravel and sand. In the remaining five catchments we sampled one grain size, sand. Our analysis provided erosion rates of 15 to 26 mm Ky^{-1} for the 0.025 to 0.050 cm sand samples and 12 to 20 mm Ky^{-1} for 3 to 8 cm gravel samples. We analyzed these TCN measurements in the context of several basin metrics, including slope and relief, derived from a digital elevation model (DEM). Our results provide evidence that most surficial basin metrics are not good predictors of denudation rates at a global scale, but can aid in predictions at a regional level. This finding supports the dynamic equilibrium hypothesis of landscape evolution and casts doubt on the possibility to estimate basin-wide denudation rates and watershed sediment supply at a global scale from simple metrics of basin morphology.

CHAPTER 1

INTRODUCTION

In order to understand the life cycle of a mountain range, researchers must identify and quantify the processes that influence the rate of denudation and sediment flux through landscapes in a variety of settings. While numerous studies using modern methods have focused on denudation rates in tectonically active regions (e.g., Pratt-Sitaula et al., 2004; Wobus et al., 2005, Belmont et al., 2007; Densmore et al., 2009; Stock et al., 2009), relatively few researchers have investigated tectonically inactive orogens (e.g., Heimsath et al., 2001; Matmon et al., 2003).

Landscape Evolution Models

The questions relating to the persistence of long-lived orogens are themselves long-lived. The most prominent early theory was that of Davis' (1889). He proposed a geographic cycle in which landscapes are uplifted, then incised and gradually eroded over time to a relatively flat surface, or peneplain, at which time the cycle repeats. Davis realized renewed tectonics would interrupt this cycle and the "penultimate plain" would be a feature rarely, if ever, found in landscapes (Pazzaglia, 2003).

Davis' theory was later replaced by Hack's (1960) "dynamic equilibrium" which suggested that a landscape will adjust its form to attain relatively uniform erosion and retain its overall character as long as the processes operating on it remain constant. The dynamic equilibrium theory infers that relief and the distribution of hillslope gradients will remain unchanged in a steady-state system. Hack believed all landscapes are a reflection of the modern processes acting on them. His central concept provides that

summits of resistant rock types result in steeper slopes compared to less-resistant rocks. These steeper slopes would theoretically allow for denudation of the more resistant rocks to keep pace with the lower-resistant rocks with less-steep slopes. The result is the entire landscape lowering at the same rate. Hack recognized changes in both tectonics and climate can disrupt this equilibrium.

In contrast, Ahnert (1970) proposed a linear relationship between relief and denudation suggesting that steady-state relief is unattainable in Hack's "dynamic equilibrium". Based on an empirical equation he derived from large mid-latitude drainage basins, it would take approximately 18.5 My to lower relief to ten percent of its initial value in cases with isostatic rebound.

River Basin Morphometric Analysis

There have been several previous attempts to use digital elevation model (DEM) derived metrics - slope, relief, hypsometry, to model denudation rates and other geomorphic processes (von Blanckenburg, 2005; Roering et al., 2007; Portenga and Bierman, 2011). The basis for such modeling requires a correlation between these metrics and measured denudation rates.

Although researchers have come to a consensus on the timing of uplift of the Appalachians (Thomas, 2006; Hatcher, 2010), little is known about the rates and processes influencing the subsequent erosion of this orogen. Previous studies have estimated denudation rates for the core of the Appalachians ranging between 4 to 57 mm/ky (e.g., Hancock and Kirwin, 2007; Judson and Ritter, 1964; Matmon, et al., 2003, Portenga and Bierman, 2011). Offshore basins provide evidence of approximately 7 km of crustal section from the Appalachians being deposited during the past 180 My (Poag

and Sevon, 1989). We expand on these studies by searching for correlations between DEM-derived topographic metrics and millennial-scale denudation rates calculated using in situ-produced terrestrial cosmogenic nuclide (TCN) measurements of Beryllium-10 (^{10}Be) from ten basins selected in the southern Appalachians (Figure 1).

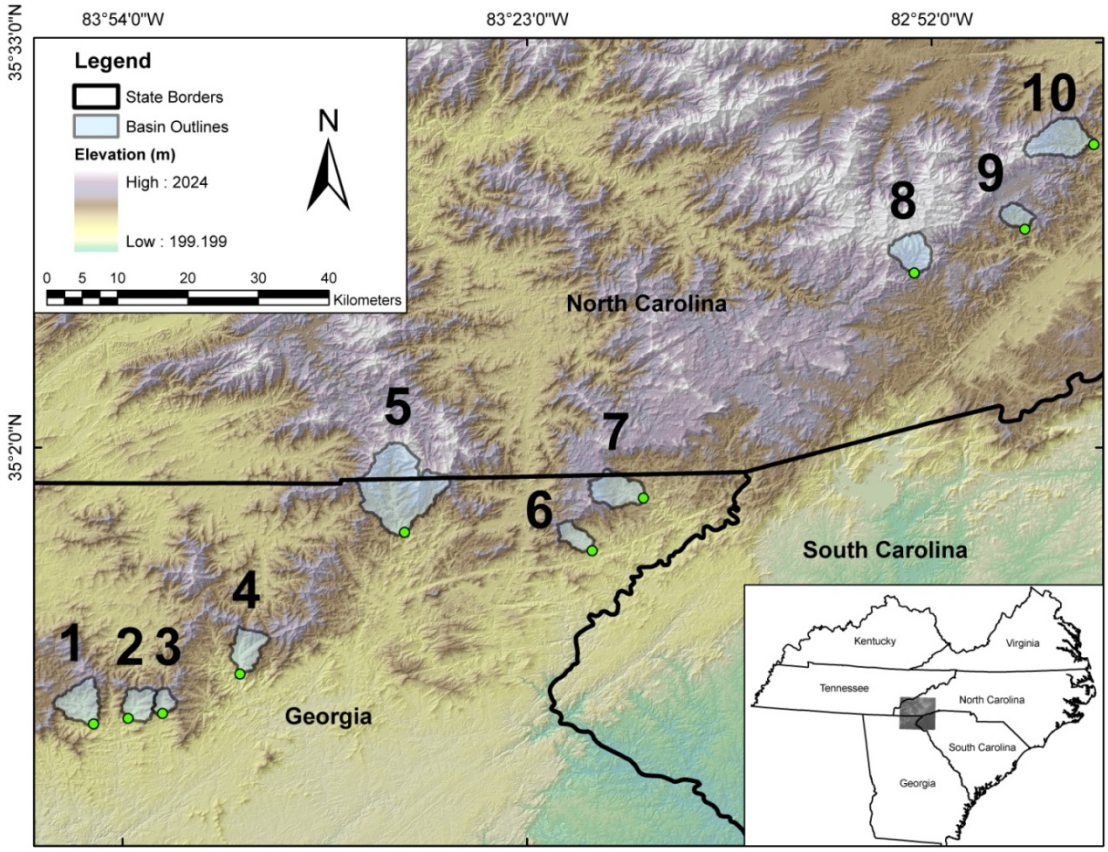

Figure 1. Topographic map of southern Appalachians. Locations of ten basins are shaded in light blue with sample collection locations identified in green. Sand samples were collected at all ten basins. Gravel samples were collected at basins 1, 4, 6, 8, and 10. A large area between basin 7 and 8 was eliminated from site selection due to significant development in the Highlands and Cashiers areas of North Carolina.

Cosmogenic Nuclides

While the geology, climate, and various basin metrics are useful in creating models to explain the geomorphic processes occurring within a catchment, these models are calibrated to current features in the landscape (hillslope gradient, relief, average precipitation, etc). As such, they may be useful in understanding the current sediment dynamics but provide little information on longer timescales. Using cosmogenic nuclides, we can directly measure denudation rates averaged over the entire basin over 10^3 -10^6 year timescales. Prior results provide rates of 10^4 -10^5 year timescales for denudation rates of the Appalachians (Hancock and Kirwin, 2007; Judson and Ritter, 1964; Matmon, et al., 2003). TCN geochronology is an excellent tool to measure rates of geomorphic processes (Lal, 1991; Granger et al., 1996; Gosse and Phillips, 2001; Bierman and Nichols, 2004; von Blanckenburg, 2006; Willenbring and von Blanckenburg, 2010).

Understanding TCN processes of production and delivery, and geomorphic processes that contribute to their distribution and concentration at the Earth surface is required for sample collection, analysis and data interpretation. A number of studies show the usefulness of ^{10}Be in measuring basin-wide denudation rates (Brown et al., 1995; Granger et al., 1996; Matmon et al., 2003; Bierman and Nichols, 2004; von Blanckenburg, 2006) and sediment transport mechanisms within the landscape (Belmont et al., 2007). The abundance of the target mineral, quartz, in a variety of rock types and geographic settings, contributes to ^{10}Be's widespread usefulness among TCNs. Quartz is highly resistant to chemical weathering and provides stoichiometric simplicity.

Beryllium-10 production rates in quartz are exceptionally well constrained, making it an ideal target mineral for TCN analysis (Gosse and Phillips, 2001; Dunai, 2010).

Two types of ^{10}Be are found in the natural environment: ‘meteoric’ and ‘in situ’. Meteoric ^{10}Be is produced in the atmosphere and delivered to the Earth’s surface through precipitation (see comprehensive review by Willenbring and von Blanckenburg, 2010). In situ ^{10}Be is produced inside the mineral grains of sediment within the top meter of the Earth’s surface. Both are generated by high-energy cosmic radiation reacting with a target nucleus (silicon and oxygen in quartz), shattering the nucleus of the atom. The TCN is produced as a byproduct of this reaction. Within the scope of this work we focus on only in situ ^{10}Be and all references to ^{10}Be or TCNs below refer to this type.

TCN production rates vary with latitude and elevation. As atmospheric pressure decreases, cosmic ray attenuation decreases (Stone, 2000). At higher latitudes and at higher altitudes the atmospheric column is shorter, resulting in lower atmospheric pressure. As a result, higher latitudes and altitudes experience higher production rates.

The production rate of ^{10}Be also decreases exponentially with depth below the surface at a rate that primarily depends on regolith/rock density. Therefore, in an actively eroding landscape, the concentration of ^{10}Be is indirectly proportional to the rate at which sediment is exhumed and eroded from the landscape. Low concentrations of ^{10}Be indicate rapid erosion rates and high concentrations of ^{10}Be indicate slow erosion rates. The timescale over which a ^{10}Be basin-average erosion rate integrates is approximately equal to the time it takes to erode one attenuation length (typically ~ 90 cm) of the exponential decay function of the production rate.

Recent studies suggest that concentrations of TCNs in varying grain sizes can provide important information about sediment source to sink pathways (Brown et al, 1995; Niemi et al., 2005; Belmont et al., 2007). However, some basic questions remain regarding how geomorphic processes influence the surface exposure history of, and therefore the TCN concentrations in, alluvial sediment. As a result, there exists a critical need to study how watershed erosion and sediment transport histories affect the TCN concentrations in alluvium, and hence, the interpretations of denudation rates and surface exposure ages derived from these data sets. To further our understanding of these processes, we analyze ^{10}Be concentrations in two alluvial sediment grain sizes to investigate the geomorphic processes responsible for eroding and transporting sediments from hillslopes, through drainage networks, and ultimately to sedimentary depocenters.

Our study included ten basins within the Blue Ridge escarpment of the southern Appalachian Mountains. We collected both sand (0.025-0.050 cm) and gravel (3-8cm) from five active channels for analysis of ^{10}Be concentrations in the two distinct grain sizes. A single grain size (sand, 0.025-0.050 cm) was collected in the remaining five basins.

Beryllium-10 was extracted from quartz minerals provided in each sample and analyzed using Accelerator Mass Spectrometry (AMS). AMS provides precise measurement of trace amounts of ^{10}Be extracted from geologic samples. Using these measurements we can calculate the concentration of ^{10}Be in our sample and determine the basin-wide denudation rate (Vermeesch, 2007).

Research questions

Our research focuses on the following questions: 1) What are the millennial-scale rates of denudation in a post-orogenic landscape and how do they compare to millennial-scale denudation rates measured in tectonically active landscapes? 2) Are denudation rates dependent on relief, as Ahnert (1970) suggests, or on any other topographic metrics? and 3) Do different alluvial grain size fractions exhibit similar or different TCN concentrations? In either case, what are the implications for our understanding of watershed erosion and sediment transport processes?

CHAPTER 2

GEOLOGIC SETTING

The formation of the Appalachians began during the Paleozoic when the eastern Laurentian margin was created by the breakup of supercontinent Rodinia 750 My. Three main orogenies formed the Appalachians: arc accretion during the Taconic orogeny, 470 to 440 My; north-south, transpressional collisions during the Acadian orogeny, 380 to 360 My; and the final north-south, transpressional, and head-on collision of the previous orogenies with Gondwana upon completion of Pangea during the Alleghanian orogeny, 380 to 270 My (Hatcher, 2010).

There is also some indication of an even earlier orogen that involved tectonic accretion during the Grenville orogeny, 1350 to 1000 My. Thomas (2006) outlines evidence for two complete Wilson cycles contributing to the creation of the Appalachians. A Wilson cycle is a sequence of events relating to the opening and closing of an ocean basin, and the corresponding breakup or formation of a continent.

The two Wilson cycles related to the Appalachians are the closing of an ocean to create the supercontinent Rodinia, the opening of the Iapetus Ocean when Rodinia breaks apart, the closing of the Iapetus Ocean to create Pangea, and the opening of the Atlantic Ocean when Pangea breaks apart. Evidence suggests the ancient Appalachians had initial relief of 3.5 to 4.5 km (Slingerland and Furlong, 1989).

The Blue Ridge escarpment is hypothesized to have originated, and continues to migrate westward, as a result of long-term erosional processes (Pazzaglia and Gardner,

2000; Spotila et al., 2004). The escarpment is approximately 800 km long, reaching from northern Georgia to the Virginia-Maryland border, and ranges 300-600 m in height.

Ten basins along the east-draining Blue Ridge escarpment in the southern Appalachians were selected for this study. All ten study basins are primarily underlain by quartz-rich gneiss and schist (Figure 2; Dicken et al., 2005), thus minimizing the effect of lithology on denudation rates. Additional localized areas of quartz-rich granite, quartzite, and quartz diorite occur in and around the basins. While areas of non-quartz bearing metamorphic rocks (e.g. gabbro, mafic gneiss, marble and slate) occur in the study area, these all appear on the western side of the continental divide or well below the drainage basins on the eastern side, thus any contribution of these lithologies to the samples collected is considered insignificant.

Mean annual rainfall for the Southern Appalachians varies annually between 55 and 90 centimeters (U.S. Geological Survey, National Atlas: Mean Annual Precipitation 1961-1990, http://seamless.usgs.gov/). Climate has multiple, competing effects on millennial-scale denudation rates (von Blanckenburg, 2006). Precipitation and temperature influence denudation directly through water run-off and freeze-thaw processes, and indirectly by supporting vegetation and wildlife that can both restrict denudation and contribute via tree-throw, bioturbation, and other processes.

Most of the study area is protected National Forest land, providing a well preserved setting in which to investigate natural denudation processes. While much of the southern Appalachians has seen logging activities in the past, areas with high slopes like the basins in our study are impractical for timber harvesting and the cost prohibitive

access makes logging both present and past unlikely (Southern Appalachian Man and the Biosphere, 1996).

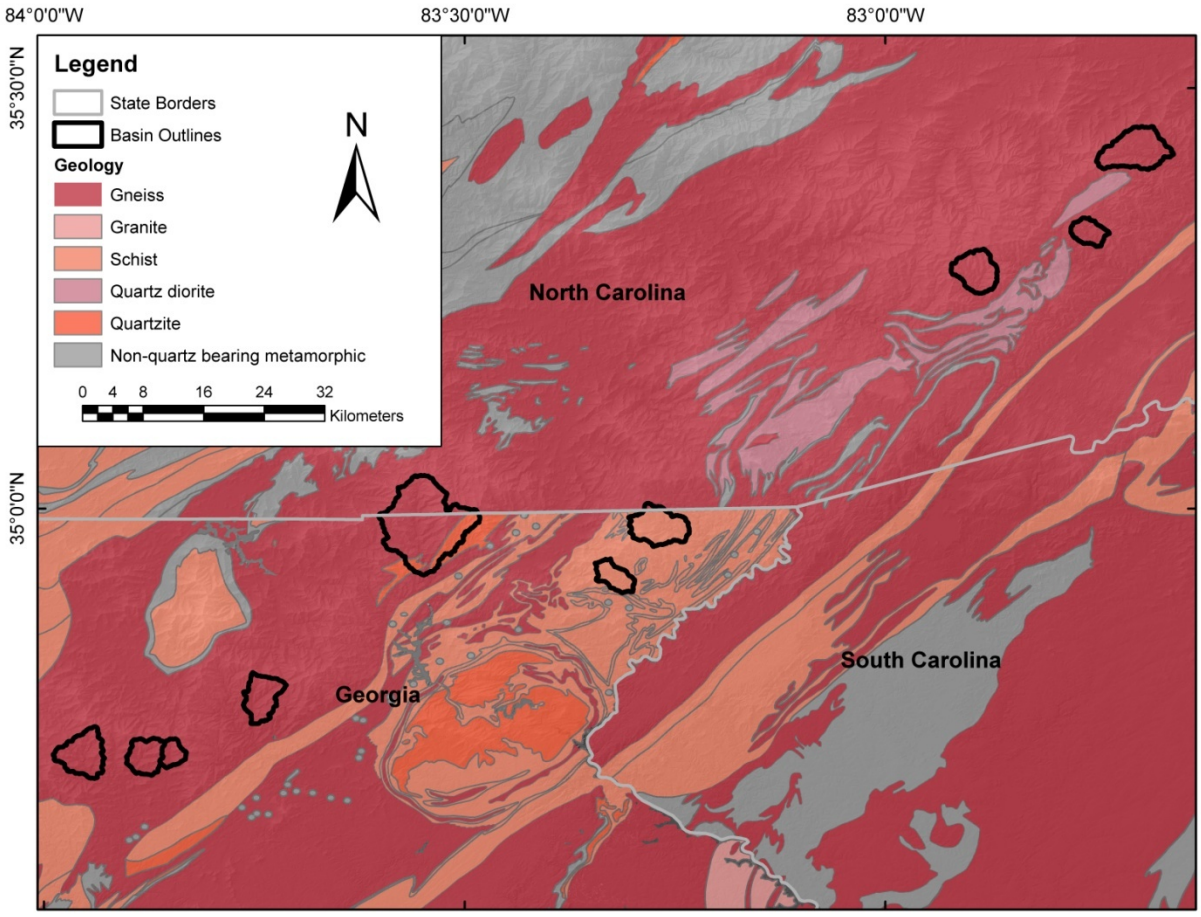

Figure 2. Geologic map of study area with sample basins outlined in black. All ten basins are underlain by quartz-rich gneiss and schist (Dicken et al., 2005), thus minimizing the effect of lithology on denudation rates. Additional localized areas of quartz-rich granite, quartzite, and quartz diorite occur in and around the basins. Larger areas of non-quartz bearing metamorphic rocks (e.g. gabbro, mafic gneiss, marble and slate) occur in the study area; however these all appear on the western side of the continental divide or well below the drainage basins on the eastern side, and thus any contribution these lithologies might make to the samples would be considered insignificant.

CHAPTER 3

METHODS

Site selection

Locations for sample collection were initially identified using National Elevation Dataset (NED) 1/3 arc second data in ArcGIS 9.1, overlain with geologic data (Dicken et al., 2005) and National Atlas data of landslides and dams from the U.S. Geological Survey (http://seamless.usgs.gov/).

Several factors went into determining sample locations. The most important factors were size of basin, availability of quartz-rich lithologies, absence of landslides, and absence of pervasive human influences. Numerous basins of approximately 25 km^2 in size along the Blue Ridge escarpment were selected using the NED and other datasets. Nearly the entire escarpment is comprised of quartz-rich lithologies necessary for ^{10}Be TCN geochronology analysis (Figure 2).

Landslides can activate the movement of sediment that hasn't been exposed to cosmogenic nuclides, resulting in distorted TCN measurements (Niemi, et al., 2005; Yanites et al., 2009). Specifically, landslides contribute large pulses of sediment with anomalously low TCN concentrations, which would suggest erroneously fast denudation rates. At larger basin scales, the stochastic effects of individual landslides can be averaged out (Binnie et al., 2006). However, to avoid this potential problem, the basins selected for this research were specifically chosen to exclude landslide dominated areas.

Sample collection points were selected to minimize localized human impacts, which could dramatically increase erosion and/or sediment storage in the watershed upstream. For example, all sample sites were located more than a kilometer upstream of

any dams in the channel system so sediment storage within the system is not controlled by human-made grade control structures. Satellite imagery compiled by Google Maps (maps.google.com) was also consulted to determine if any land development occurred upstream. A large area between basins seven and eight was eliminated from selection due to significant development in the Highlands and Cashiers areas of North Carolina (Figure 1).

In the field, we further investigated the watershed area upstream of the collection point, both by vehicle and by foot, to verify there was limited or no development and or other factors that could result in distortion of TCN measurements; for example, recently erected bridges built over the active channel, paved or gravel roads, farm land or homes, evidence of past logging activities, etc. In many cases this involved traveling a dirt road that ran parallel to the active channel to its end near the ridgeline. Basins with significant development were eliminated from our selection. Significant development was defined as more than 15 homes or buildings within the basin. Any development or factor that could contribute to TCN distortion was recorded in our field notebooks for further consideration.

Additional factors of grain sizes available contributed to our sample selection while in the field. In some areas only sand sizes were available, in others only gravel sizes. Basins with sand only, or sand and gravel were used. We did not select basins that provided only gravel in our study. Sand was sampled from the active channel in all ten basins. Gravel samples were collected from the same locations as sand in basins 1, 4, 6, 8, and 10.

A sample of active channel alluvium collected at any given point within a catchment is assumed to be an aggregate of grains originating from every part of the watershed upstream of that point. Each grain has eroded from a different location within the catchment and has followed a slightly different transport pathway, with mixing occurring as the grains move down hillslope and downstream. In this way, each grain arrives at our sample location with a unique surface exposure history. The aggregate of these exposure histories, each represented in proportion to the rate at which their point of origin is eroding, yields the basin-average erosion rate. We sampled our basin as far downstream in the catchment as possible to include a large variety of grains. Spatially-averaged denudation rates can be calculated using the following equation:

$$N = \frac{P_0 \Lambda}{E}$$

where N is the ^{10}Be concentration, P_0 is the production rate (latitude/altitude corrected and adjusted for shielding), Λ is the attenuation length (approximately 90 cm for most soil types), and E is erosion rate (Granger et al., 1996).

We used the CosmoCalc excel add-in which provides tools utilizing the above equation (cosmocalc.googlepages.com; Vermeesch, 2007). CosmoCalc provides denudation rates using a single TCN based on inputs of TCN concentration, TCN concentration uncertainty, and a combined production rate correction factor which includes latitude/altitude corrections and shielding factors.

Sample Processing

For sand samples, approximately three kilograms of material was collected and brought back to the Georgia Institute of Technology's Frankel Cosmogenic Geochronology Laboratory. Sand samples were sieved to a range of 0.025 to 0.050

centimeters. For gravel size samples (ranging from 2 to 8 cm diameter), approximately 80 to 100 grains were collected, crushed, amalgamated, ground, and sieved to a range of 0.025 to 0.050 centimeters.

For both sand and gravel samples, quartz was purified using a series of dilute hydrofluoric (HF) and nitric (HNO_3) acid treatments in heated, ultrasonic tanks. The first HF treatment was at 7.5 g/L of 1% HF and 1% HNO_3, two subsequent treatments were at 15 g/L of the same concentration. Each treatment was run for nine hours. Typical samples require three of these acid treatments for purification leaving only the highly resistant quartz remaining.

While the gravel size samples were typical in terms of mineralogy, the sand samples collected were more complicated. Specifically, sand samples were found to be high in garnet and the HF treatment was not efficient at removing this mineral. In these cases an additional step using heavy-liquid mineral separations solution with a density of 2.85 g cm^{-3} and a fourth HF treatment was added.

This HF process serves to remove any meteoric ^{10}Be from the sample in addition to removing other mineral types. Visual inspection is sufficient to verify the sample contents are purified quartz.

Beryllium-10 was extracted from approximately 75 grams of purified quartz for each sample (Table1). Beryllium-9 carrier is added to the weighed out sample and the process blank to serve as the nuclide of known quantity for AMS analysis. The process blank is put through exactly the same steps as the samples in order to determine if any meteoric ^{10}Be is contributed from the atmosphere during sample processing.

The quartz (with added carrier) is initially dissolved in concentrated HF and dried over approximately 24 hours in a fume hood. Each sample is then fumed three times with perchloric acid to convert fluorides to perchlorates and is dried between each fuming. The sample is then put through ion exchange chromatography to remove titanium, iron, and aluminum from the Be. The remaining Be fraction is dried, redissolved in a 50% hydrochloric acid (HCl), 50% water (H_2O) mixture. All mixtures of water involved the use of deionized and purified water. The water was purified using a nanopure filtration system.

Beryllium was precipitated out of the HCl/H_2O mixture using ammonium hydroxide. The precipitated gel was then dried and ignited at 750 C for five minutes to convert the beryllium hydroxides to oxides (Bierman et al., 2002). The resulting beryllium oxides were then mixed with Niobium powder and transferred to stainless steel targets for analysis by accelerator mass spectrometry at the Lawrence Livermore National Laboratory – Center for Accelerator Mass Spectrometry (LLNL-CAMS).

Measured $^{10}Be/^{9}Be$ ratios were converted to ^{10}Be concentrations following Balco (2006) and adjusted for process blanks. A total of four process blanks were analyzed with these specific samples. We also included one previous blank and three subsequent blanks, all of which were analyzed by LLNL-CAMS.

Beryllium-10 Production Rate Scaling

To interpret the cosmogenic nuclide concentrations in terms of a denudation rate, the TCN production rate must be estimated. There are several estimated normalized sea-level high-latitude (SLHL) production rates from the literature (e.g.: Lal, 1991; Stone,

2000; Dunai 2001; Desilets & Zreda, 2003; Desilets et al. 2006). These SLHL production rates must be adjusted based on the location of samples collected.

Cosmic ray attenuation decreases as atmospheric pressure decreases (Stone, 2000). As a result, higher latitudes and altitudes experience higher production rates. Topography can also influence production rates (Gosse and Phillips, 2001). In the same way that mountains shield (or shade) the adjacent landscape from solar radiation, topographic features can shield the Earth's surface from cosmic rays. Additional shielding is possible from thick and long-term snow cover. While snow is common in the highlands of the southern Appalachians, its effects were considered negligible. Snow depths of >50 cm for four months of the year are required to produce noticeable reductions in attenuation of cosmic rays (Gosse and Phillips, 2001). Snow depth lasting more than a few days is uncommon in the study area (http://www.nohrsc.noaa.gov).

For the sake of computational efficiency, we resampled the 1/3 arc second (10 by 10 meter) DEM obtained from the U.S. Geological Survey to a 50 by 50 meter DEM to calculate production rate scaling factors for each cell in the DEM. The production rate scaling factor includes altitude and latitude corrections and topographic shielding adjustments (Appendix A).

We ran the production rate calculation procedure using both the higher resolution and lower resolution DEMs on two of the smaller basins (3 and 9) to determine the computational efficiency and examine whether or not this resampling introduces any undesirable artifacts. While computing time was reduced by more than half, there was no noticeable difference in the computed basin-average production rates.

There is no consensus regarding the most accurate SLHL TCN production rate for ^{10}Be. For this reason, all five production rates (Lal, 1991; Stone, 2000; Dunai 2001; Desilets & Zreda, 2003; Desilets et al. 2006) provided by CosmoCalc (Vermeesch, 2007) were used to calculate basin-wide denudation rates for each basin. These generally accepted production rates range from 4.95 to 5.19 atoms g^{-1} yr^{-1}.

Basin Morphology Analysis

Basin metrics were calculated using the 10-meter DEM data from seamless.usgs.gov and tools available in ArcGIS 9.1 and ArcINFO 9.1. We extracted a drainage basin file from our larger DEM file using the procedures outlined in Appendix B. With this smaller drainage basin file, we extracted and analyzed relief, mean hillslope gradient, hypsometry, elongation index, basin size, and volume to area ratio. Details on how we extracted each of these metrics is outlined in Appendix B. We provide summary information here.

Relief is defined as the difference between maximum elevation and minimum elevation within each drainage basin as shown in Figure 1. Higher relief within a basin of a given size would suggest steep slopes. As such, one would anticipate a correlation between relief and denudation rates to be similar to a correlation between slope and denudation rates. The ‘describe’ function in ArcINFO provided maximum and minimum elevations allowing us to calculate relief.

We used ArcINFO’s ‘slope’ command to calculate the slope for each grid cell in our basin files. Slope is defined as the rate of change of each grid cell compared to its eight neighboring cells and is calculated in degrees. Using the ‘describe’ function on a slope file provides the maximum, minimum, and mean slope in degrees.

Drainage basin hypsometry describes the distribution of elevations throughout a watershed. A useful attribute of hypsometry is that drainage basins of different sizes can be compared with each other because area and elevation are plotted as normalized functions of total area and total elevation. We used a simplified hypsometric integral (HI) calculation (Brocklehurst and Whipple, 2004).

$$HI = \frac{mean\ elevation - minimum\ elevation}{maximum\ elevation - minimum\ elevation}$$

Basin elongation is defined as the maximum length divided by the maximum width. In ArcMap, we used the 'Measure distance and area' tool to find the maximum length (measured along the most prominent stream) and maximum width (measured perpendicular to the most prominent stream) of each drainage basin. Basins with an elongation index of approximately 1 would tend to be more circular. All other morphological attributes held constant, circular basin morphology causes more rapid convergence of streamflow because all points are closer to the watershed outlet, relative to a basin with elongation significantly greater or less than 1 but of the same areal coverage. More rapid convergence of flow to the drainage basin mouth could potentially result in relatively higher peak flows and therefore a higher erosion rate.

Basin size was calculated using the same data provided by basin elongation measurements. A larger basin size would have a larger drainage basin area upstream from the sample. A greater drainage basin area would lead to higher streamflow which could increase denudation rates, but larger drainage areas also tend to contain more areas for sediment storage, which would tend to reduce denudation rates, so the effects of drainage basin area are not expected to be unequivocal.

The basin volume to area (V/A) ratio is a metric that indicates the degree of dissection in a landscape. The volume of rock eroded is normalized to the basin area. Like hypsometry, it is useful when comparing basins of different sizes. A larger V/A ratio would suggest more erosion within the landscape compared with a basin exhibiting a lower V/A ratio. As such, one would expect a correlation between V/A ratios and denudation rates.

Basin metrics were analyzed against one another to determine if correlations exist between metrics. We used R^2 values to indicate if one or more metrics were providing duplicate information about their influences on erosion rates.

$$R^2 = \left[\frac{\sum(x-\bar{x})\,(y-\bar{y})}{\sqrt{\sum(x-\bar{x})^2 \sum(y-\bar{y})^2}}\right]^2$$

Regression analysis was performed on each of the basin metrics. The regression residuals were then compared, using R^2 values, to the basin metrics to determine if a given metric might contribute to the variance provided by the regression analysis.

A p-value indicates whether or not a correlation is statistically significant or if it might be appearing by chance. We calculated p-values using the same data as our R^2 values. Usually a p-value of 0.05 or lower suggests the result we have is statistically significant. But based on our very small sample size, we have lowered our acceptable p-value to 0.001.

Longitudinal profiles of a channel can provide information on knickpoints, channel steepness and concavity. The basis for this analysis comes from the concept that channel slope decreases as a power function of upstream drainage area following:

$$S = kA^{\theta}$$

where S is the local channel slope, A is upstream contributing drainage area, k is the steepness of the channel profile and θ is concavity of the channel profile. Concavity is the rate of decrease of slope in the downstream direction.

The longitudinal profile can identify where anomalously steep or flat areas exist. These areas could be indicative of focused erosion in the case of steep areas or knickpoints or knickzones, or areas of deposition in the case of flat areas.

Gallen et. al (2011) suggests a link between upstream migration of knickpoints and steepened hillslopes. These steepened hillslopes would provide greater potential energy and thereby a faster erosion rate. Visual inspection of long profiles as well as numerical analysis can provide additional details on the locations of knickpoints both upstream and downstream of our collection site.

River channel networks were identified and extracted using the 'Flow direction' and 'Flow accumulation' tools in ArcGIS. The flow accumulation output provides each grid cell with a numerical value indicating the number of grid cells up-watershed that contribute flow to that point, based on flow direction output. We then selected all cells with values greater than 1000 as our stream network. This equates to a drainage area threshold of approximately 100,000 m^2. Main trunk channels were then isolated and river longitudinal profiles were extracted.

The data extracted provides "elevation steps", the number of units an elevation occurs over, in one meter increments. Using this data, we mathematically defined a knickzone as a location where the ratio of change in elevation to change in distance is greater than or equal to 5:1. We've used the term knickzone instead of knickpoint

because there might be instances where we find a significant change in elevation of a distance larger than what would be considered a knickpoint.

CHAPTER 4

RESULTS

Landscape characteristics

Our field work provided an opportunity to visually inspect the landscape. All of the basins consistently exhibited heavy vegetation and hillslopes of soil-mantled colluvium. Bedrock outcrops were seen in streams, but rarely on hillslopes or ridgelines. Evidence of diffusive erosion processes: tree throw, soil creep, bioturbation, can be found throughout the study area (see basin photos in Appendix C).

Table 1 provides information related to development occurring upstream of our sample collection sites. If upstream development was a factor influencing the denudation rate results, one would expect the results for basins 3, 4, and 5 to produce outliers in our results. Removal of these three basins did not reduce scatter in our graphs or significantly change any R^2 values. This suggests the minimal amount of development upstream did not influence our results.

Terrestrial Cosmogenic Nuclides

The denudation rates computed for each basin using all the five different SLHL production rates (Lal, 1991; Stone, 2000; Dunai 2001; Desilets & Zreda, 2003; Desilets et al. 2006) provided by CosmoCalc (Vermeesh, 2007), resulted in differences of less than 1% within each basin, indicating that production rate models are generally in good agreement in this part of the world. All results and any corresponding figures were calculated using a SLHL production rate of 5.13 atoms g^{-1} yr^{-1} (Lal, 1991). Table 2 provides calculated shielding factors and calculated production rates for each basin.

Table 1. Development information on basins

Basin	Additional information
1	No development upstream, dirt road.
2	No perminant development, group campsite located upstream, dirt road.
3	Several homes upstream, paved road parallels stream.
4	Few houses upstream, paved road parallels stream.
5	Approximately 5 miles upstream of sample site is Tate City, pop. 32 ±. Several houses and buildings. Remainder of basin is undeveloped. Paved roads throughout basin.
6	No development upstream, dirt road.
7	No development upstream, dirt road.
8	No development upstream, dirt road.
9	No development upstream, dirt road.
10	No development upstream, dirt road.

In five of the ten catchments (basins 1, 4, 6, 8, and 10), we sampled two grain sizes, gravel and sand. In the remaining five catchments (basins 2, 3, 5, 7, and 9), we sampled only one grain size, sand (Figure 1, Table 2).

For four of the five basins tested with two grain sizes, higher ^{10}Be concentrations were found in the gravel samples as compared to the sand samples (Table 3, Figure 3a). These higher concentrations translate to lower denudation rates for four of the five gravel samples as compared to the sand samples analyzed (Figure 3b). Four gravel size erosion rates provided differences of 7.2, 6.7, 5.0 and 3.1 mm Ky^{-1} slower than the sand samples, while one gravel size erosion rate was 2.0 mm Ky^{-1} faster than the sand sample. Our overall results provided basin-average erosion rates between 15 to 26 mm Ky^{-1} (with an

Table 2. Methodological Data for Terrestrial Cosmogenic Nuclide ^{10}Be Geochronology

Basin Number	Sample	Type of Sample	Shielding and Scaling Factor[a]	Production Rate[b] (atoms g^{-1} yr^{-1})	Quartz (g)	Be carrier[c] (g)
1	BR-0210-01	sand	1.69	8.69	72.8489	0.3122
	BR-0210-02	gravel			74.9892	0.3122
2	BR-0210-03	sand	1.67	8.59	75.0201	0.3135
3	BR-0210-04	sand	1.74	8.94	75.0347	0.3112
4	BR-0210-05	sand	1.71	8.79	75.1566	0.3080
	BR-0610-11	gravel			74.9712	0.3055
5	BR-0210-06	sand	2.04	10.44	75.0359	0.3047
6	BR-0210-07	sand	1.67	8.58	75.0914	0.3057
	BR-0610-12	gravel			75.3753	0.3117
7	BR-0610-21	sand	1.82	9.34	74.6921	0.3098
8	BR-0410-08	sand	2.51	12.87	65.9733	0.3096
	BR-0410-09	gravel			75.0056	0.3051
9	BR-0410-10	sand	1.97	10.13	75.1090	0.3049
10	BR-0610-15	sand	2.06	10.56	74.7591	0.3108
	BR-0610-16	gravel			75.1354	0.3092

[a]Shielding and scaling factor is a combination of the latitude/altitude correction and topographic shielding factor.
[b]Production rate is 5.13 atoms g^{-1} yr^{-1} [Lal, 1991] adjusted for shielding and scaling factor.
[c]Be carrier concentration is 1354 mg mL^{-1}.

Table 3. Analytical Results of Terrestrial Cosmogenic Nuclide ^{10}Be Geochronology

Basin Number	Type of Sample	Location[a] °N/°Wb	Altitude (m above sea level)	Grain Size[b] (cm)	$^{10}Be/^{9}Be$[c,d] (x 10-13)	Measured ^{10}Be[d,e,f] (10^5 atoms/g SiO_2)	Denudation Rate[g] (mm/kyr)
1	sand	34.68031 / 83.93708	575	.0250-.0500	7.52 ± 0.33	2.91 ± 0.13	20.12 ± 0.94
	gravel	34.68031 / 83.93708	575	6-8	11.84 ± 0.32	4.45 ± 0.13	12.91 ± 0.39
2	sand	34.68757 / 83.89297	544	.0250-.0500	9.81 ± 0.17	3.70 ± 0.08	15.49 ± 0.33
3	sand	34.69379 / 83.84902	591	.0250-.0500	7.47 ± 0.32	2.79 ± 0.12	21.51 ± 0.99
4	sand	34.74429 / 83.75000	529	.0250-.0500	6.23 ± 0.29	2.30 ± 0.11	25.89 ± 1.29
	gravel	34.74421 / 83.75011	529	4-8	8.37 ± 0.23	3.08 ± 0.09	19.18 ± 0.59
5	sand	34.92509 / 83.53985	597	.0250-.0500	7.97 ± 0.55	2.92 ± 0.20	23.76 ± 1.72
6	sand	34.90152 / 83.30022	680	.0250-.0500	7.22 ± 0.16	2.65 ± 0.06	21.86 ± 0.55
	gravel	34.90232 / 83.30090	680	3-4	9.11 ± 0.17	3.40 ± 0.07	16.89 ± 0.38
7	sand	34.96874 / 83.23481	643	.0250-.0500	9.14 ± 0.21	3.42 ± 0.09	18.16 ± 0.47
8	sand	35.25595 / 82.88883	900	.0250-.0500	8.41 ± 0.14	3.56 ± 0.07	23.59 ± 0.46
	gravel	35.25595 / 82.88883	900	4-6	11.14 ± 0.29	4.09 ± 0.11	20.46 ± 0.59
9	sand	35.31185 / 82.74751	790	.0250-.0500	7.00 ± 0.19	2.56 ± 0.08	26.41 ± 0.81
10	sand	35.42010 / 82.65945	740	.0250-.0500	10.55 ± 0.19	3.96 ± 0.08	17.53 ± 0.37
	gravel	35.42010 / 82.65945	740	3-4	9.62 ± 0.32	3.57 ± 0.12	19.50 ± 0.71

[a]In most cases both grain sizes were collected at the same location and time. Basin 4 and 6 are exceptions. The gravel size was collected on a second visit to the site.

[b]Sizes provided are in diameter range

[c]Isotope ratios were normalized to 10Be standards prepared by Nishiizumi et al. [2007] with a value of 2.85×10^{12} and using a ^{10}Be half-life of 1.36×10^{6} years.

[d]Uncertainties are reported at the 1σ confidence level.

[e]A mean blank value of 76,421 ± 26,940 ^{10}Be atoms ($^{10}Be/^{9}Be = 2.709 \times 10^{-15} \pm 9.54 \times 10^{-16}$) was used to correct for

[f]Propagated uncertainties include error in the blank, carrier mass (1%), and counting statistics.

[g]Beryllium-10 denudation rates were calculated with the CosmoCalc Excel add-in [Vermeesch, 2007] version 1.8

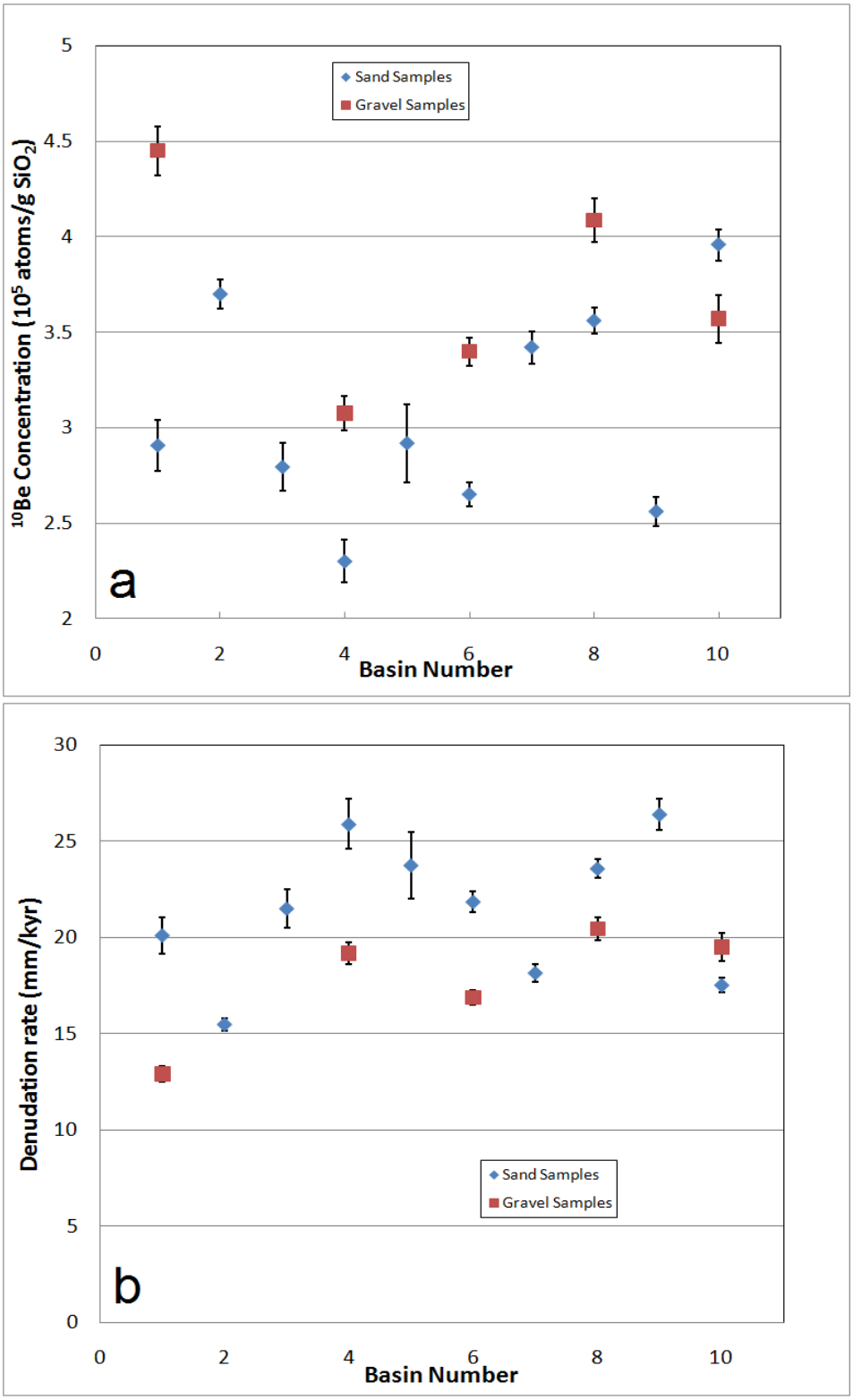

Figure 3. Terrestrial cosmogenic nuclide results providing ^{10}Be concentrations (3a) and denudation rates (3b). Blue diamonds indicate sand samples, red squares indicate gravel samples, and error bars are shown in black.

average of 21.4 mm Ky^{-1}) for the 0.025 to 0.050 cm sand samples and 12 to 20 mm Ky^{-1} (with an average of 17.8 mm Ky^{-1}) for 3 to 8 cm gravel samples (Table 3, Figure 3b).

Basin Metrics

The ten basins investigated provide maximum elevations ranging from 1134 meters in basin 6 to 1828 meters in basin 8, with an average maximum elevation of 1391 meters. Minimum elevations range from 488 meters in basin 4 to 920 meters in basin 8, with an average minimum elevation of 620 meters. Topographic relief within the ten study basins varies between 602 meters in basin 3 and 1079 meters in basin 5, with average relief of 771 meters. Mean slope angles range between 17^{o} to 26^{o}. Table 4 provides minimum, maximum and mean elevations and topographic metrics investigated for each basin. It also shows averages and standard deviations for each of these categories. Items in bold indicate values that are outside the range of one standard deviation above the mean and items shaded in gray indicate values that are outside the range of one standard deviation below the mean. Items outside of two standard deviations are in dashed boxes.

Table 4: Topographic metrics

Basin	Min elevation (m)	Max elevation (m)	Mean elevation (m)	Total Relief (m)	Mean Slope (degrees	Hypometric Integral (%)	Elongation (m/m)	Basin Area (km^2)	Volume to Area (m^3/m^2)
1	520	1355	789	835	21.2	32	1.03	31	51
2	510	1175	762	665	21.9	38	1.29	18	52
3	571	1173	823	602	23.3	**42**	1.45	10	**60**
4	488	1225	792	737	23.1	**41**	1.77	24	52
5	596	**1675**	1004	**1079**	23.1	38	1.23	**140**	54
6	521	1134	729	613	19.2	34	**2.20**	12	41
7	630	1433	885	803	17.8	32	1.49	30	40
8	**920**	**1828**	**1288**	908	**25.3**	40	1.18	28	**59**
9	729	1306	961	577	24.0	40	1.34	11	53
10	713	1610	1018	897	23.5	34	1.44	45	52
Average	620	1391	905	772	22.2	37	1.44	35	51
Standard Deviation	135	240	169	163	2.3	4	0.33	38	7

Values greater than the range of one standard deviation are displayed in bold, values lower than the range of one standard deviation are displayed in gray shading. Items in dashed boxes fall outside of two sandard deviations.

Figure 4 shows each of the basin metrics investigated- relief (a), mean slope (b), hypsometric integral (c), elongation (d), basin area (e), and volume to area (f), regressed against basin-average denudation rates. Most of the basin metric plots look very similar - fairly consistent scatter and no extreme outliers. The one graph showing a clear outlier is basin area in which basin 5 is significantly larger than the other basins (Figure 4e).

Figure 5 shows index maps with corresponding long profiles of each of our ten basins. Long profiles are shown in matching colors to index maps with sand-size denudation rates basins included. Sample collection locations are indicated with black dots on graphs. Dams occurring along profile are noted with pink and only occur along the profile for basin 5 (Figure 5b). The profile graphs are vertically exaggerated to provide greater detail.

Our intention was to trace the long profiles to the point at which they all intersected downstream. But many of our streams flowed into lakes rather than one river or stream. As such, the long profiles were traced until they reached the elevation of a common lake they fed into, or to a common point in a river or stream. Basins 1 through 4 all feed into Lake Lanier in north Georgia. Basins 5 through 7 all feed into Lake Hartwell which sits along the border of Georgia and South Carolina. Basins 8 through 10 all met in North Carolina's French Broad River just south of Ashville, North Carolina.

These streams all exhibit relatively smooth, concave-up graded stream profiles with the few exceptions. Basin 5 has four dams located below the collection point (indicated by the ~ 6 km long relatively flat reach just downstream from the sample site and ending with an abrupt dropoff, which is the location Tallulah Falls dam and Tallulah

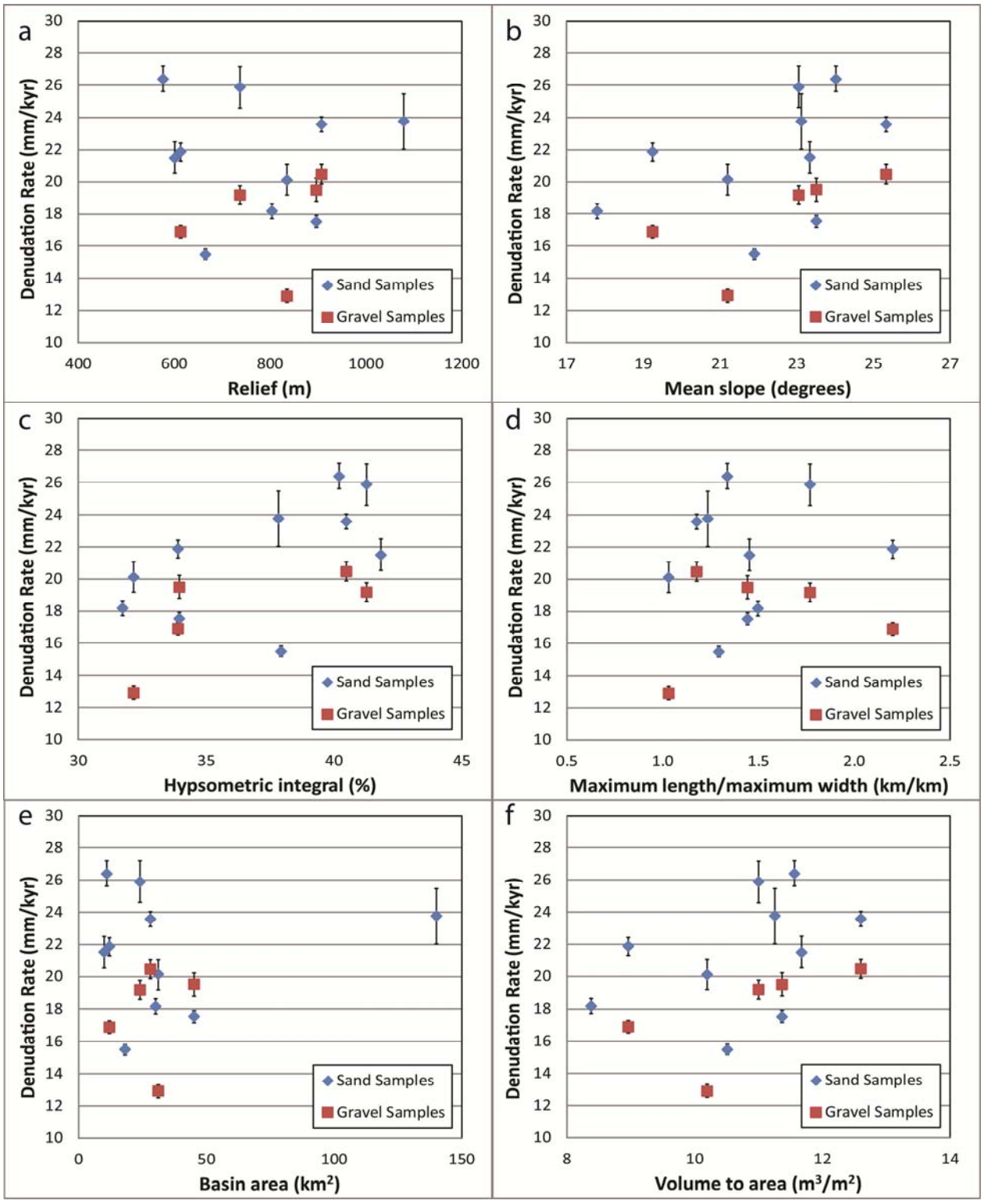

Figure 4. Basin metrics versus denudation rates. Graphs show relief (a), mean hillslope gradient (b), hypsometric integral (c), elongation (d), basin area (e) and volume to area (f) with sand samples in blue, gravel samples in red, and error bars in black.

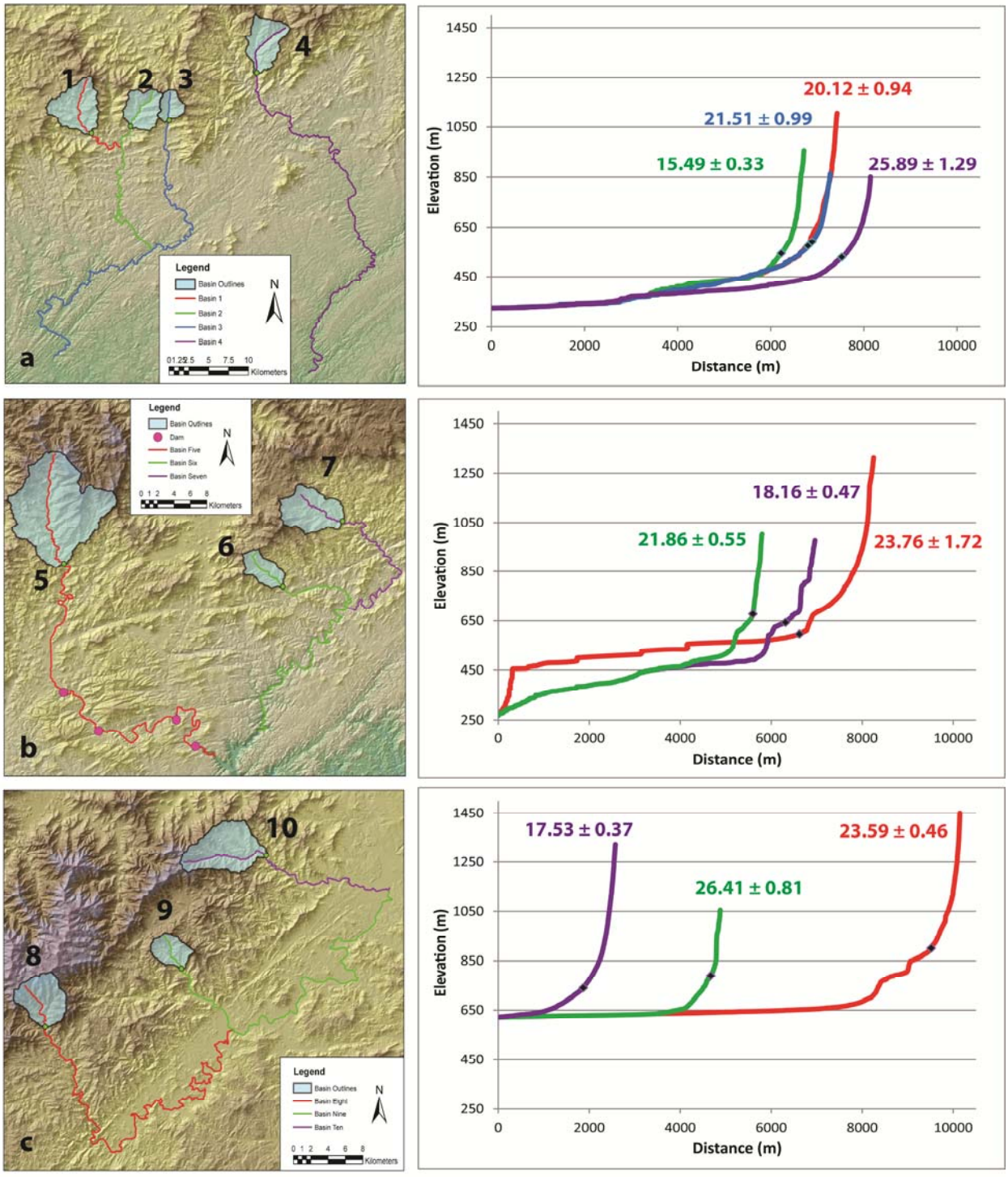

Figure 5. Topographic maps with corresponding long profiles of basins 1 through 4 (a), 5 through 7 (b), and 8 through 10 (c). Long profiles are shown in matching colors to index maps with denudation rates displayed. Sample locations are indicated with black dots on graphs. Dams occurring along profile are noted with pink and only occur along the profile for basin 5 (b)

Gorge; Figure 5b) disrupting what would otherwise likely be a graded profile. This stretch of the profile is comprised of several man-made lakes created by hydroelectric dams.

There are indications of possible knickpoints, or knickzones, upstream of the sampling locations for basin 5 and 7 and downstream of the sampling location for basin 6, 7, and 8.

Tables 5 and 6 show the R^2-values and p-values for the metrics analyzed. Items shaded in gray are considered statistically insignificant based on a p-value greater than our threshold of 0.001. Items in bold indicate a correlation based on R^2 values greater than 0.5000 and a p-value of less than our 0.001 threshold.

Combining all of these results, we provide some evidence on what basin metrics can be used to estimate denudation rates.

Are any of these metrics auto-correlated?

Do any of the metrics tell us the same information? The first section of table 5 and table 6 shows R^2 values and p-values for basin metrics regressed against one another to determine if/how any of them are correlated, and therefore provide overlapping pieces of information. Our results show that mean slope and volume to area are strongly correlated (R^2=0.9850), indicating they are likely providing duplicate information.

Do any of these metrics provide correlations to denudation rates?

The second section of table 5 and table 6 provide R^2 values and p-values for denudation rates versus our six basin metrics. Using the sand samples alone (top row of Table 5b; n=10) and the sand and gravel samples (third row from the top of Table 5b; n=15) we see no correlation between our basin metrics and denudation rates. The highest

correlation value is given by hypsometry (R^2=0.3376 and R^2=0.3434, respectively). Using just the gravel samples (second row of Table 5b; n=5) we see a moderate correlation between hypsometry and denudation rates (R^2=0.5104). When we average the sand and gravel results for the five basins where we have two grains size samples (fourth row of Table 5b; n=5), we find a very high correlation between hypsometry and denudation rates (R^2=0.9279).

Does one metric explain the variance produced by another metric?

Each of our basin metrics produced a significant amount of variability. Using regression analysis for each of the metrics, we can calculate residuals to determine if any of the other metrics would be able to account for the variability seen in the primary relationships.

For regression analysis to provide adequate information, it would require that the metric being regressed have some sort of correlation to the factor it is being regressed against. The second section of Table 5 and Table 6 suggests only regression analysis on hypsometry could provide statistically valid information based on R^2 values greater than 0.3000. However, we went ahead and performed the analysis on each metric.

Section three of Table 5 and Table 6 shows the results of a second order regression (using residuals) for sand samples (n=10). The fourth section shows the results of second order regression analysis for gravel samples (n=5). The fifth section of these Tables shows the results of second order regression analysis with the averages of our denudation rates for the five basins for which we have two grain sizes. No significant secondary correlations exist with the sand faction denudation rates. Residuals of the

Table 5. R^2 values

a

Basin Metric	Relief	Mean Slope	Hypsometry	Elongation	Basin Area	V/A
Relief	-	0.0322	0.0541	0.2058	**0.6915**	0.0369
Mean Slope	-	-	**0.5570**	0.1846	0.0182	**0.9850**
Hypsometry	-	-	-	0.0044	0.0068	**0.5624**
Elongation	-	-	-	-	0.0907	0.2204
Basin Area	-	-	-	-	-	0.0181
V/A	-	-	-	-	-	-

b

Denudation rates	Relief	Mean Slope	Hypsometry	Elongation	Basin Area	V/A
Sand	0.0020	0.1970	0.3376	0.0182	0.0112	0.1673
Gravel	0.0593	0.4724	**0.5104**	0.0355	0.0259	0.4220
All rates	0.0006	0.1813	0.3434	0.0064	0.0205	0.1632
Average rate	0.0056	0.2732	**0.9279**	0.0807	0.0900	0.2361

c

Regression Residual: Sand Samples	Relief	Mean Slope	Hypsometry	Elongation	Basin Area	V/A
Relief	0.0000	0.2046	0.3262	0.0131	0.0205	0.1748
Mean Slope	0.0194	0.0000	0.0777	0.1320	0.0026	0.0012
Hypsometry	0.0123	0.0002	0.0000	0.0453	0.0356	0.0011
Elongation	0.0003	0.2565	0.3544	0.0000	0.0218	0.2273
Basin Area	0.0178	0.1867	0.3516	0.0281	0.0000	0.1577
V/A	0.0183	0.0017	0.0903	0.1284	0.0031	0.0000

d

Regression Residual: Gravel Samples	Relief	Mean Slope	Hypsometry	Elongation	Basin Area	V/A
Relief	0.0000	0.2538	**0.5045**	0.1732	0.0023	0.2103
Mean Slope	0.1857	0.0000	0.1353	**0.6340**	0.1006	0.0023
Hypsometry	0.0585	0.1011	0.0000	0.0491	0.1621	0.0874
Elongation	0.1733	**0.6540**	**0.5162**	0.0000	0.0836	**0.6070**
Basin Area	0.0118	0.3643	**0.5646**	0.0884	0.0000	0.3208
V/A	0.1543	0.0028	0.1683	**0.5961**	0.0724	0.0000

e

Regression Residual: Average of Sand and Gravel Samples	Relief	Mean Slope	Hypsometry	Elongation	Basin Area	V/A
Relief	0.0000	0.3416	**0.9481**	0.0482	0.0565	0.3019
Mean Slope	0.3410	0.0000	**0.5344**	0.4641	0.4913	0.0017
Hypsometry	0.4236	0.1503	0.0000	**0.7939**	0.2611	0.1708
Elongation	0.0332	**0.5089**	**0.9818**	0.0000	0.0142	0.4744
Basin Area	0.0354	**0.5286**	**0.9151**	0.0086	0.0000	0.4712
V/A	0.3018	0.0020	**0.5740**	0.4441	0.4305	0.0000

Items in bold indicate correlations greater than 0.5000. Items shaded in gray considered statistically insignificant according to calculated p-value greater than 0.001.

Table 6. P-values

a

Basin Metric	Relief	Mean Slope	Hypsometry	Elongation	Basin Area	V/A
Relief	-	1.45E-07	1.72E-07	1.15E-07	**7.05E-08**	1.28E-07
Mean Slope	-	-	**3.68E-08**	1.95E-10	3.27E-01	**1.19E-09**
Hypsometry	-	-	-	2.64E-10	8.59E-01	**4.58E-10**
Elongation	-	-	-	-	2.26E-02	5.74E-10
Basin Area	-	-	-	-	-	7.88E-02
V/A	-	-	-	-	-	-

b

Denudation rates	Relief	Mean Slope	Hypsometry	Elongation	Basin Area	V/A
Sand	1.43E-07	5.54E-01	2.56E-08	2.52E-08	2.99E-01	2.25E-06
Gravel	1.46E-04	2.70E-02	**7.31E-05**	2.20E-04	1.29E-01	4.11E-03
All rates	1.02E-11	7.51E-02	1.60E-12	1.37E-11	1.55E-01	4.90E-08
Average rate	1.48E-04	1.19E-01	**1.84E-04**	5.48E-05	2.01E-01	3.62E-04

c

Regression Residual: Sand Samples	Relief	Mean Slope	Hypsometry	Elongation	Basin Area	V/A
Relief	1.12E-07	4.26E-11	1.84E-14	2.41E-01	1.87E-02	2.10E-06
Mean Slope	1.12E-07	5.04E-12	1.44E-14	1.94E-01	1.87E-02	5.58E-07
Hypsometry	1.12E-07	8.09E-13	1.83E-14	1.57E-01	1.87E-02	1.55E-07
Elongation	1.12E-07	3.63E-11	1.76E-14	2.37E-01	1.87E-02	1.91E-06
Basin Area	1.12E-07	3.89E-11	1.79E-14	2.38E-01	1.87E-02	1.99E-06
V/A	1.12E-07	7.20E-12	1.44E-14	2.02E-01	1.87E-02	7.03E-07

d

Regression Residual: Gravel Samples	Relief	Mean Slope	Hypsometry	Elongation	Basin Area	V/A
Relief	1.34E-04	1.47E-06	**7.82E-07**	3.23E-01	5.18E-03	4.00E-04
Mean Slope	1.34E-04	2.82E-07	2.38E-06	**1.99E-01**	5.60E-03	4.47E-05
Hypsometry	1.34E-04	2.61E-07	2.77E-06	1.85E-01	5.65E-03	3.28E-05
Elongation	1.34E-04	**1.61E-06**	**7.49E-07**	3.18E-01	5.13E-03	**4.28E-04**
Basin Area	1.34E-04	1.68E-06	**7.38E-07**	3.20E-01	5.12E-03	4.42E-04
V/A	1.34E-04	3.24E-07	1.97E-06	**2.15E-01**	5.54E-03	6.47E-05

e

Regression Residual: Average of Sand and Gravel Samples	Relief	Mean Slope	Hypsometry	Elongation	Basin Area	V/A
Relief	1.34E-04	4.68E-07	**1.41E-06**	2.48E-01	5.43E-03	1.23E-04
Mean Slope	1.34E-04	2.64E-07	**2.69E-06**	1.88E-01	5.64E-03	3.48E-05
Hypsometry	1.35E-04	9.05E-06	3.02E-05	**4.10E-03**	6.25E-03	4.79E-06
Elongation	1.34E-04	**3.84E-07**	**1.66E-06**	2.31E-01	5.49E-03	9.01E-05
Basin Area	1.34E-04	**3.75E-07**	**1.69E-06**	2.29E-01	5.49E-03	8.66E-05
V/A	1.34E-04	2.78E-07	**2.43E-06**	1.97E-01	5.61E-03	4.28E-05

Items shaded in gray considered statistically insignificant due to preset threshold of 0.001. Items in bold indicate R2 values of greater than 0.500

relationships between basin metrics and denudation rates derived from gravel samples exhibit some significant correlations. When the residuals from the basin metric versus denudation rates averaged between sand and gravel are considered, hypsometry appears to explain a significant amount of the variability observed in the other relationship, again suggesting that hypsometry is tightly linked to the processes controlling basin-wide denudation rates over millennial timescales.

Do the answers to any of our above questions change if we remove outliers?

While removal of the three basins showing higher occurrences of development did not reduce scatter in our graphs, removing basin 4 did increase our R^2 values for correlations between average denudation rates of the two grain sizes and basin metrics. It also increased our p-values suggesting these results are no longer significant, likely due to a smaller sample size (n=4).

Two basins (6 and 8) provided five occurrences of falling outside of one standard deviation in the various categories show on Table 4. Removing either or both of these basins provided a few higher R^2 values but, once again, removing the basins increased the p-value indicating the data may be statistically insignificant.

Basins 1, 3, 4, 5, 7, and 9 all have at least one item that falls outside one standard deviation (Table 4). Removing these basins, one at a time, produced no effect on R^2 values.

Looking at it from a different perspective, we tried removing outliers from each category. For example, removing basins 5, 6, and 8 since they all fall outside of one standard deviation for maximum elevation. We continued this process of removing for all the variables shown on Table 4. In almost all instances, any increase in R^2 value was

matched with an increase in p-value, indicating a lack of statistical significance. However, there was one exception. Removing the data from basins 1 and 6 (based on the fact that they are both outliers for elongation) provided very high correlations between denudation rates for gravel and elongation and volume to area ratios (Table 7). While we question the validity of this result, these values were considered statistically significant according to p-value, even though we are now dealing with a sample size of n=3.

Table 7. R^2 values and p-values calculated after omitting basin 1 and basin 6

R^2 Value		Basin Metric					
		Relief	Mean Slope	Hypsometry	Elongation	Basin Area	V/A
Denudation rates	Sand	0.0004	0.2625	0.4259	0.0144	0.0122	0.2313
	Gravel	0.5433	0.9969	0.0315	**0.8906**	0.0090	**0.9992**
	All rates	0.0023	0.1694	0.2872	0.0000	0.0151	0.1514
	Average rate	0.3033	0.0451	0.9996	0.0315	0.9959	0.0346

P-value		Basin Metric					
		Relief	Mean Slope	Hypsometry	Elongation	Basin Area	V/A
Denudation rates	Sand	4.79E-06	4.73E-01	6.23E-07	2.17E-06	3.06E-01	9.67E-05
	Gravel	4.44E-03	1.14E-02	1.30E-02	**5.51E-05**	1.89E-01	**2.71E-04**
	All rates	1.12E-08	1.14E-01	3.09E-10	4.30E-09	1.84E-01	1.33E-06
	Average rate	4.44E-03	1.31E-01	6.39E-03	3.62E-03	2.18E-01	9.88E-03

R^2 Value		Basin Metric					
		Relief	Mean Slope	Hypsometry	Elongation	Basin Area	V/A
Regression Residual: Gravel Samples	Elongation	0.6579	**0.9705**	0.0037	0.9524	0.0005	**0.9789**
	V/A	0.4804	**0.9999**	0.0571	0.8482	0.0247	**0.9988**

P-value		Basin Metric					
		Relief	Mean Slope	Hypsometry	Elongation	Basin Area	V/A
Regression Residual: Gravel Samples	Elongation	4.21E-03	**1.15E-05**	2.02E-03	2.06E-02	3.25E-02	**7.21E-05**
	V/A	4.23E-03	**1.09E-04**	3.02E-03	8.42E-03	3.56E-02	**8.80E-05**

Items in bold indicate correlations greater than 0.5000. Items shaded in gray considered statistically insignificant according to calculated p-value of greater than 0.001.

Does the presence of knickpoints or knickzones influence denudation rates?

Table 8 shows the results of our numerical process of identifying knickzones in the long profiles. Only one basin has knickzones occurring downstream of the collection site, basin 5. Basin 5's denudation rate of 23.76 ± 1.72 (Table 3) is not considered an outlier and the occurrence of both downstream knickzones and dams does not seem to influence denudation rates in this basin.

We calculated R^2 values on the number of upstream knickzones versus denudation rates and found no correlations between the presence of upstream knickzones. Basins 9, 4, and 5 have the highest sand denudation rates of 26.41 ± 0.81, 25.80 ± 1.29, and 23.76 ± 1.72, respectively. Basin 9 has three small upstream knickzones, basin four has no knickzones, and basin 5 has two rather large knickzones upstream. If the presence of knickzones were a factor, we would anticipate the two basins (basins 3 and 4) without knickzones to have our lowest denudation rates. These two basins fall 5th and 9th in order from lowest to highest denudation rates. Because we extracted our longitudinal profiles from 10 m DEMs, we are only capable of observing rather large knickzones. It is possible that smaller knickzones and knickpoints may exist at a resolution lower than our analysis can detect.

Table 8. Basin Knickzones

Basin	Number of upstream knickzones	Number of downstream knickzones	Additional information
1	2	-	All small knickzones
2	1	-	All small knickzones
3	-	-	None
4	-	-	None
5	2	3	Two large upstream knickzones and 4 dams downstream
6	7	-	Five of these occur in a 14 meter distance but breaks between prevent us from counting them as one knickzone
7	6	-	One large upstream knickzone, all others are small
8	6	-	One large upstream knickzone, all others are small
9	3	-	One large upstream knickzone, all others are small
10	3	-	All small knickzones.

Small knickzones are defined as occuring over less than 5 meters distance

CHAPTER 5

DISCUSSION

Cosmogenic Nuclide Denudation Rates

Our ^{10}Be concentrations provided basin-wide denudation rates within a relatively narrow range of between 15 to 26 mm Ky^{-1} (average 21.4 mm Ky^{-1}) for the 0.025 to 0.050 cm sand samples and 12 to 20 mm Ky^{-1} (average 17.8 mm Ky^{-1}) for 3 to 8 cm gravel samples (Table 3, Figure 3b). The rates integrate over the past 10^4 years. These estimated denudation rates are internally consistent and fall within the range of denudation rates (4 to 57 mm Ky^{-1}) produced by other recent studies throughout the Appalachians (Matmon et al., 2003; Portenga and Bierman, 2011).

The range of results suggests the landscape of the Appalachians has been fairly uniformly over the past 10^4 to 10^5 years. This slow and spatially consistent denudation process suggests the Appalachians have likely held their current shape over hundreds of thousands of years and will continue to do so as a result of isostatic uplift. These results support the dynamic equilibrium hypothesis of landscape evolution in the Appalachians as suggested by Hack (1960). Ahnert's (1970) theory of a mountain belt losing up to ninety percent of its relief in 18.5 My is in stark contrast to our results.

Morphometric Indices and Denudation Rates

Hyposometry

The results from regression analyses indicate that hypsometric integrals provide the highest correlations with our denudation rates (Table 5 and 6). Using only the gravel

samples (basins 1, 4, 6, 8, and 10; n=5), we see a moderate correlation between hypsometry and denudation rates (R^2=0.5104). Using only the sand samples (n=5) for these same five basins, we see a stronger correlation between hypsometry and denudation rates (R^2=0.6898) compared to the results using all ten basins (n=10, R^2=0.3376).

Gravel was collected from every channel it was available. These five basins have some fundamental difference within them that enabled their denudation processes to provide gravel size grains where the other samples collection sites did not. We do not have enough data to determine what contributes to this difference. Reviewing figure 4 suggests the five basins with gravel samples are evenly distributed among the other five basins with respect to relief, hillslope gradient, basin area, elongation, hypsometric integral, and volume to area ratio.

If we average the two grain sizes for the five basins for which we have two samples sizes (n=5), we find an even higher correlation between the hypsometric integral and denudation rates (R^2=0.9279). This high correlation suggests that averaging rates from multiple grain sizes may provide more useful information regarding the links between basin morphology and watershed erosion and sediment transport processes than do either of the single grain sizes independently.

Stepwise multiple regression analysis showed that none of the other metrics explained the variance in relationship between hypsometry and sand size grains, gravel size grains, or grain-averaged denudation rates. However, the hypsometric integral appeared to explain some significant portion of the variance between grain size-averaged denudation rates and several other morphometrics. This further suggests that the

hypsometric integral is a key basin characteristic factoring into denudation rates on millennial timescales.

Drainage basin hypsometry describes the distribution of elevations throughout a watershed. The resulting curves can identify three stages of maturity (Strahler, 1952). The early youth, or inequilibrium, stage is indicated by a hypsometric integral greater than 60%. The mature, or equilibrium, stage is indicated by a hypsometric integral between 35% and 60%. The monadnock, or old age, stage is indicated by an abnormally low hypsometric integral (less than 35%). This monadnock stage is usually the result of significant differences in rock resistance types within a drainage basin resulting in a large area of low elevation of weaker resistant lithologies compared with a relatively small area of high elevation comprised of stronger lithologies.

For discussion purposes, when we discuss the age or stage of a basin as it relates to hypsometry, we are referring to that stage of its landscape and equilibrium. We are not referring to actual ages in terms of timescales. When we say "older", we mean more in equilibrium, rather than geologically older. When we say "younger", we are referring to a basin that is farther from reaching equilibrium.

Because we find similar lithologies throughout the study area, we would not expect to find a drainage basin of the monadnock stage, however four of our basins (basins 1, 6. 7. and 10) fall within this upper limits of the monadnock stage, according to Strahler (1952), while six of our basins (basins 2, 3, 4, 5, 8 and 9) are considered mature, or equilibrium, stage. We consider all of our basins to be in an equilibrium, or mature, stage. However, there appears to be a distinct break between the two stages represented by our basins (Figure 4c), which occurs at Strahler's more rigidly defined stages.

A basin with a high hypsometric integral would be characterized as having a larger portion of its area represented by high elevations (in a relative sense within that watershed) and a small portion of its area represented by low elevations as a result of recent incision of the channel network that has not yet propagated up through the hillslopes. A basin with a low hypsometric integral would be characterized as having greater area at lower elevations. We could also conclude these basins would have larger areas with lower relief.

The mechanistic link between hypsometric integrals and erosion rates likely relates to the potential energy gradients and distribution of mass within the watershed. For example, a basin exhibiting a high hypsometric integral would have more mass available to near-channel erosional processes and greater potential energy gradients to drive erosion due to the higher elevations and higher relief near the channel network. In contrast, basins exhibiting a low hypsometric integral have relatively greater area occurring at lower, and presumably flatter, elevations providing more space for sediment storage and reducing the probability that high potential energy gradients come into contact with high kinetic energy near-channel erosion processes.

Elongation

Basin elongation is the maximum length divided by the maximum width. Our study basins exhibited a range of elongation between 1.03 and 2.20, with two points falling outside of one standard deviation. Eliminating basins 1 and 6 from our data set due to their anomalous elongation indices provided very high correlations for our gravel size samples (Table 7). R^2 values of 0.8906 and 0.9992 for basin metrics elongation and volume to area, respectively. Our small sample size makes the statistical robustness

questionable, but the very high R^2 values suggest that a basin's shape could be linked to denudation rates.

We also note that the gravel size fraction shows a near linear trend in relief, mean slope, elongation, and volume to area if one of the data points is ignored (Figure 4). The outlier data point is observed in each of these relationships (Sample BR-0210-02 from basin 1 with a denudation rate of 12.91 ± 0.39 mm Ky^{-1}), suggesting that there may be a fundamental difference in erosion or transport of coarse material in this basin relative to the other basins studied (Figure 4). The only distinct characteristic of this basin is its elongation, which is anomalously low (1.03), suggesting its shape consists of a width that is almost equal to its length.

Removing the basin 1 data point from our gravel data set (n=4), we have R^2 values for denudation rates versus relief, mean hillslope gradient, elongation, and volume to area of 0.8527, 0.9990, 0.9343, and 0.9897, respectively. These high correlations suggest that certain basin metrics might correlate well with basins of certain elongations, but not nearly circular basins with elongations approaching the value of 1, like our basin 1.

In a basin that is nearly circular, we would expect a main trunk channel to be significantly shorter. This would result in the majority of our streamflow occurring in the smaller tributaries, thereby not providing the stronger stream power needed to move our larger gravel sizes. This distinction may play a factor in denudation rates for gravel samples, but our small sample size (n=4) makes this difficult to determine.

With the exception of basin 1 (with elongation equal to 1.03) our results suggest that more circular basins erode faster than elongate basins (Figure 4d). All other

morphological attributes held constant, the more circular basin morphology causes more rapid convergence of streamflow because all points are closer to the watershed outlet, relative to a basin with greater elongation but of the same areal coverage. More rapid convergence of flow to the drainage basin mouth tends to result in relatively higher peak flows and therefore higher stream power, consequently enabling higher gravel denudation rates.

These results suggest that for basins of certain shapes, we may be able to accurately predict a denudation rate for larger grain sizes using tools such as relief, mean slope, and volume to area.

Grain Size

The ^{10}Be concentrations in our gravel samples are systematically higher for any given basin. Of interest is how the differences between the gravel and sand ^{10}Be denudation rates decrease from basin 1 to basin 10, from southwest to northeast (Figure 3). These differences for basins 1, 4, 6, 8, and 10 are 7.2 mm Ky^{-1}, 6.7 mm Ky^{-1}, 5.0 mm Ky^{-1}, 3.1 mm Ky^{-1}, and -2.0 mm Ky^{-1}, respectively. This observation raises the question: 'what does this systematic trend tell us about transitions in erosional processes from southwest to northeast?' Our assumption is that this trend is driven by slight changes in climate as we move from southwest to northeast, but we lack sufficient data to determine this.

Many studies involving multiple grain sizes indicate that sand sized particles often contain higher concentrations of ^{10}Be than gravel sized particles (Brown et al., 1995; Matmon et al., 2003). There are two possible explanations for this (Belmont et al., 2007). The first is that gravel sizes may be transported to the channel via landslides,

which contribute large amounts of sediment from deeper in the soil profile, including gravel; that has not previously been exposed at the surface and therefore has not been dosed by cosmic radiation (Brown et al., 1995). In such watersheds, the sand-sized material is transported to the active channel via landslides, as well as slower, diffusive (hillslope creep) processes, resulting in longer surface exposure and higher ^{10}Be concentrations relative to the gravel. Our higher ^{10}Be concentrations in gravel as well as our exclusion of basins with landslide activities rules out Brown et al.'s (1995) hypothesis.

Another possible explanation for relatively higher concentrations in sand compared with gravel has been suggested by Matmon et al. (2003). Their research was conducted in a part of the Great Smoky Mountains that does not erode by landslide processes. They suggested that gravel in the active channel was likely contributed from lower elevations on the hillslopes, where production rates are proportionately lower because of additional topographic and atmospheric shielding from cosmic rays. They argued that gravel originating from higher parts of the hillslopes (which are exposed to higher production rates) would be broken down during hillslope transport and were therefore not present in the channels.

Other studies provide results with gravel sizes having higher ^{10}Be concentrations than sand sizes (Belmont et al., 2007). In this scenario, a possible explanation for gravel having higher concentrations requires a mixing of higher concentration sand from the hillslopes with that of lower concentration sand derived from comminution of ^{10}Be-deficient gravel as it moves down hillslopes and channels.

Our results of higher ^{10}Be concentrations in gravel samples compared to sand samples are most consistent with Matmon et al.'s (2003) and Belmont et al.'s (2007) theories.

Our initial denudation results were calculated based on our earlier stated assumption that a sample of active channel alluvium collected at any given point within a catchment is assumed to be an aggregate of grains originating from every part of the watershed upstream of that point. However, following the rationale of Matmon et al., (2003), it is plausible that gravel originating near the ridgeline does not survive hillslope transport, and therefore any gravel found in the active channel would be derived from lower elevations on the hillslopes. Our exclusion of basins with landslide activities enhances the possibility that our gravel size grains originated from lower on the hillslopes.

Following this logic, we calculated new shielding and scaling factors, production rates, denudation rates and residence times using the lower 20% percent of hillslope elevations for our gravel size samples. Table 9 shows the revised values with the original values for sand samples shaded in gray for comparison.

Figure 6 shows our revised denudation rates for gravel size grains in red with our original sand size denudation rates in blue. The adjustment in production rates resulted in slower denudation rates for the gravel samples, compared to our previous values. Using the initially derived production rates, basin 10 exhibited higher denudation rates for gravel than sand. However, with the revised production rates, all five basins where sand and gravel were collected exhibit slower denudation rates for gravel compared with sand.

Our adjusted results show our gravel size samples are eroding at rate of between 11.33 ± 0.35 to 16.90 ± 0.49 mm Ky^{-1} (Table 9).

Table 9. Modified Production Rates and Resulting Denudation Rate and Residence Time

Basin Number	Sample	Type of Sample	Elevation at collection site (m above sea level)	Max Elevation cut-off for production rate (m above sea level)	Shielding and Scaling Factor[a]	Production Rate[b] (atoms g^{-1} yr^{-1})	$^{10}Be/^{9}Be$ (x 10^{-13})	Measured ^{10}Be (10^{5} atoms/g SiO_2)	Denudation Rate[c] (mm/ky)	Minimum Residence Time for Gravel (ky)
1	BR-0210-01	sand	575	1355	1.6948	8.6943	7.52 ± 0.33	2.91 ± 0.13	20.12 ± 0.94	
	BR-0210-02	gravel	575	687	1.4769	7.5765	11.84 ± 0.32	4.45 ± 0.13	11.33 ± 0.35	60.0 ± 1.7
4	BR-0210-05	sand	529	1225	1.7139	8.7923	6.23 ± 0.29	2.30 ± 0.11	25.89 ± 1.29	
	BR-0610-11	gravel	529	635	1.4245	7.3077	8.37 ± 0.23	3.08 ± 0.09	16.15 ± 0.50	42.8 ± 1.3
6	BR-0210-07	sand	680	1134	1.6723	8.5789	7.22 ± 0.16	2.65 ± 0.06	21.86 ± 0.55	
	BR-0610-12	gravel	680	644	1.4671	7.5262	9.11 ± 0.17	3.40 ± 0.07	14.96 ± 0.34	46.0 ± 1.0
8	BR-0410-08	sand	900	1828	2.5091	12.8717	8.41 ± 0.14	3.56 ± 0.07	23.59 ± 0.46	
	BR-0410-09	gravel	900	1102	2.0501	10.517	11.14 ± 0.29	4.09 ± 0.11	16.90 ± 0.49	39.5 ± 1.1
10	BR-0610-15	sand	740	1610	2.0585	10.5601	10.55 ± 0.19	3.96 ± 0.08	17.53 ± 0.37	
	BR-0610-16	gravel	740	893	1.7474	8.9642	9.62 ± 0.32	3.57 ± 0.12	16.73 ± 0.61	40.5 ± 1.4

[a]Shielding and scaling factor is a combination of the latitude/altitude correction and topographic shielding factor.

[b]Production rate is 5.13 atoms g^{-1} yr^{-1} [Lal, 1991] adjusted for shielding and scaling factor.

[c]Beryllium-10 denudation rates and residence time (exposure ages) were calculated with the CosmoCalc Excel add-in [Vermeesch, 2007] version 1.8 (http://cosmocalc.googlepages.com/).

There is always a possibility the gravel size grains are moving slower than our denudation rates suggest, or that they are not moving at all. Eaton et al. (2003) shows a link between rainfall and measured denudation amounts resulting from a single catastrophic storm. They suggest a high intensity, low-frequency event can provide almost half of the overall denudation for a basin. These major storms create significant debris flows activating buried sediment of sand or gravel causing either to be higher or lower in concentration than the other.

A significant storm, deemed as being greater than tropical storm strength, has not reached our study area dating back to 1851, the time for which these records are available (U.S. Geological Survey, National Atlas: Historical Tropical Cyclone Tracks, http://seamless.usgs.gov/). The absence of a significant storm would provide additional evidence suggesting our gravel size grains may not be moving at all in addition to adding

confidence that landslides and debris flows have not contributed to our basin denudation rates.

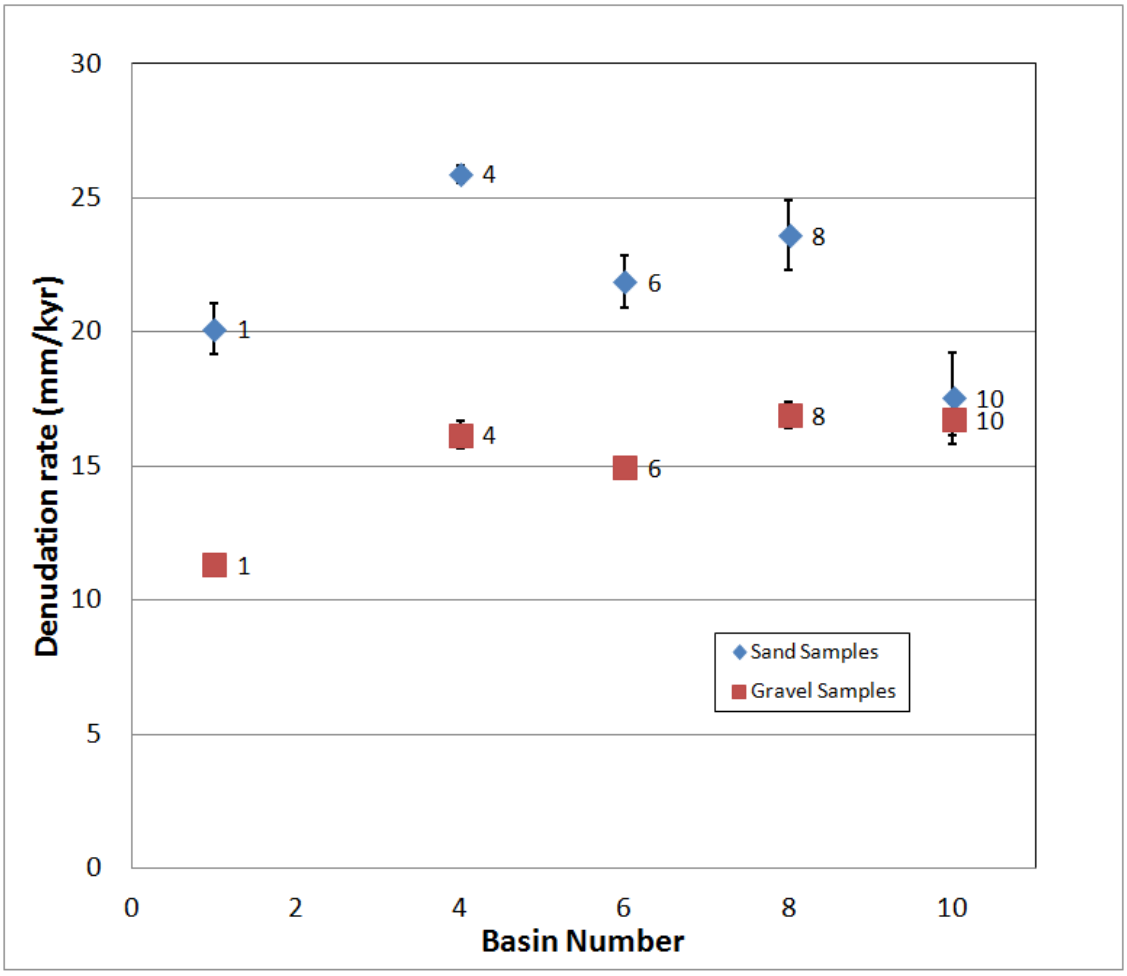

Figure 6. Revised denudation rates for gravel size samples. Revised gravel size rates shown in red, original sand size rates shown in blue, errors bars in black. Gravel size samples are now all consistently slower than sand samples.

If our grain sizes are either not moving, or are only moving as a result of high intensity, low frequency events, the steady-state assumption of our method is not appropriate and ^{10}Be concentrations measured in the gravel fraction are more indicative of gravel residence time in the system, rather than a basin-average denudation rate.

We calculated a maximum residence time based on surface exposure ages for the gravel samples using the adjusted production rates. We consider this residence time a maximum based on several assumptions. We assume the collected sample received no cosmic dosing while being un-roofed and prior to its contribution to the basin, and that we've used a reasonably accurate production rate assuming it was generated from lower on the hillslopes. In the event the sample was subjected to cosmic dosing prior to being contributed to the basin, or it came from higher elevations on the hillslope, both of these factors would require a correction resulting in a lower residence time.

The results of this analysis suggest the gravel size sediments reside in the basins at a maximum of between 39.5 ± 1.1 and 60.0 ± 1.7 Ky (Table 9).

Comparison of Denudation Rates

Portenga and Bierman (2011) compiled a global database of all publically available ^{10}Be basin-wide and outcrop denudation rates in an effort to determine how denudation rates vary over a variety of tectonic settings, climate zones and lithologies. For consistency, they standardized all results for current practices and theories related to production rates and scaling themes. Their standardization method is not an exact match to our methods, but is considered reasonably consistent for our purposes of comparison to basin-wide denudation rates.

Figures 7, 8 and 9 show denudation rates as a function of relief, slope and basin area for our samples - shown in red, as well as samples from Portenga and Bierman's database- shown in black or grey. Each data point represents a basin-wide ^{10}Be denudation rate measured in a different watershed located around the world. In cases where multiple grain size denudation rates were measured for a given basin, one data

point represents an average of the measured rates- this applies to both our samples and the database samples. For our comparisons, we only included basins from their database with areas between 1 and 3,000 km^2 for figure 7 and between 5 and 150 km^2 for figures 8 and 9.

The samples included in our comparisons have been collected from rivers and basins in Australia, Belgium, Bolivia, China, Germany, Italy, Madagascar, Spain, Sri Lanka, and the United States, and major mountain ranges such as the Coast Range, San Gabriel Mountains, San Bernardino Mountains and Appalachians in the United States, the Tibetan Plateau, Blue Mountain Plateau in Australia, and more. While there are various global locations that are not represented, an adequate sampling of settings and locations are available for our purposes (Portenga and Biermann, 2011).

Portenga and Bierman (2011) found that as they narrowed the study area, correlations between mean slope and denudation rates increased. This suggests that for regional or local scales, a stronger correlation would exist as compared to the global results. Their analyses included study areas of 8×10^2 km^2 and 7×10^4 km^2 with R^2 values decreasing from 0.75 to 0.49, respectively. Our study area is approximately 5×10^3 km^2 and produced an R^2 value of 0.20 for sand (n=10) and 0.47 for gravel (n=5). While our gravel size sample is consistent with their results, our sand sample is not. Neither of our grain size results provided p-values indicating they were statistically significant.

We selected basins ranging from 1 to 3000 km^2 located in temperate climate zones, including both tectonically active and inactive areas from Portenga and Bierman's (2011) database. Tectonically active locations were those areas with a seismicity value of

greater than 0.7000 in the database, or basins in which it is generally known that uplift is occurring, despite a seismicity value lower than 0.7000 (which was the case for three such locations in Spain and the Tibetan Plateau). Portenga and Bierman (2011) defined seismicity as "the magnitude of ground motion (peak ground acceleration) with a 10% chance of being exceeded in within 50 years."

Figure 7 shows the comparison of 366 basins in temperate climate zones with our 10 basins. Tectonically active basins are shown in black, tectonically inactive basins are shown in grey, and our study basins are shown in red. Readily apparent in figure 7 is the notion that tectonics is a primary driving force of millennial scale denudation rates, based on the significantly greater denudation rates in tectonically active regions. Denudation rates in tectonically inactive regions (Figure 7, shown in grey and red) are significantly slower.

While some researchers have found a correlation between basin metrics and denudation rates for tectonically active areas (von Blankenburg 2006), R^2 values calculated for the global dataset (0.0759, 0.2844, and 0.0003 for relief, slope and basin area respectively) indicate that any correlations are likely location or region specific and do not apply to the global rates we've included here.

We then selected samples from the Portenga and Bierman (2011) database with tectonic and climate settings similar to the southern Appalachians. Eighty-two samples collected from basins located in temperate climate zones and having seismicity values less than 0.7000 are compared to our ten basins in Figure 8.

The figure shows our denudation rates (in red) are consistent with other seismically inactive, temperate climate basins throughout the world (in grey). Again, R^2

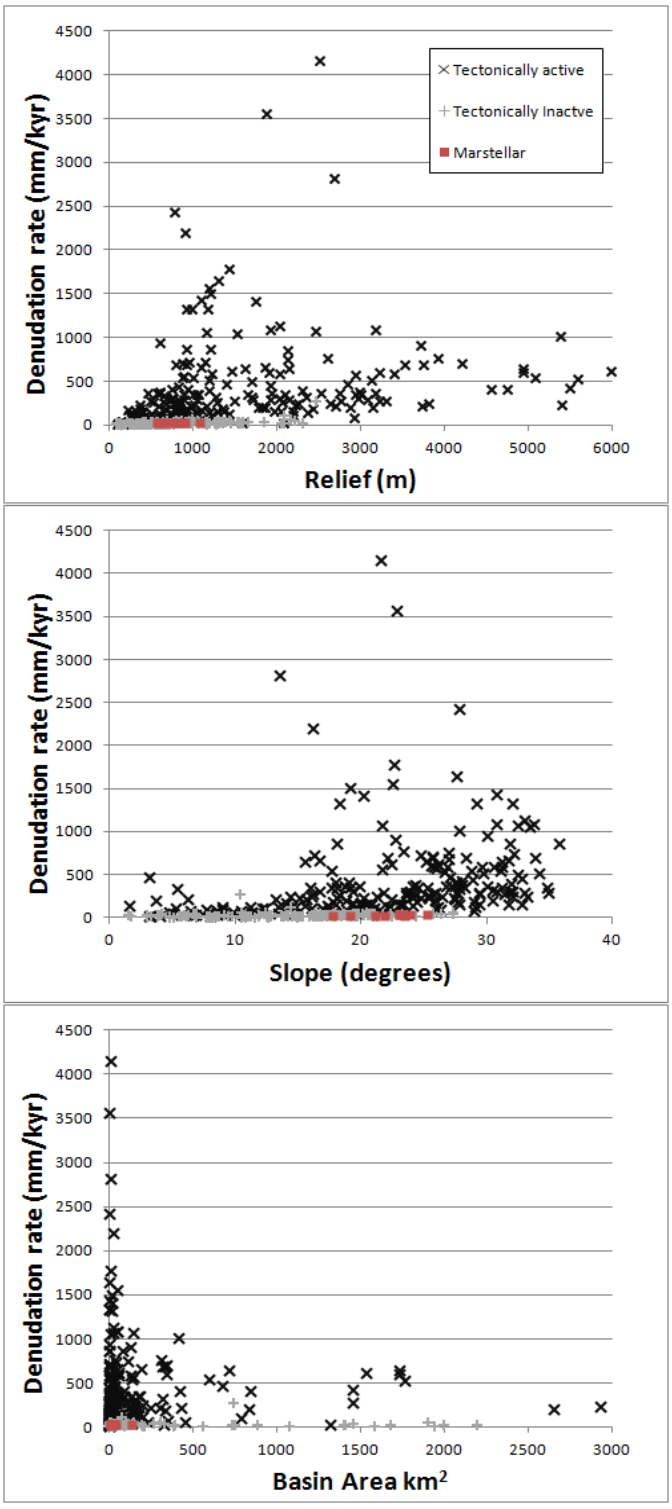

Figure 7. Comparison of Denudation rates with both Tectonically Active and Inactive locations in Temperate Climate Zones. Basin metrics versus denudation rates for tectonically active and inactive samples. Samples with a seismisity value greater than 0.700 or in a known tectonically active area were considered tectonically active. All others were considered tectonically inactive. Relief (a), mean slope (b), and basin area (c) are shown. See text for additional descriptions.

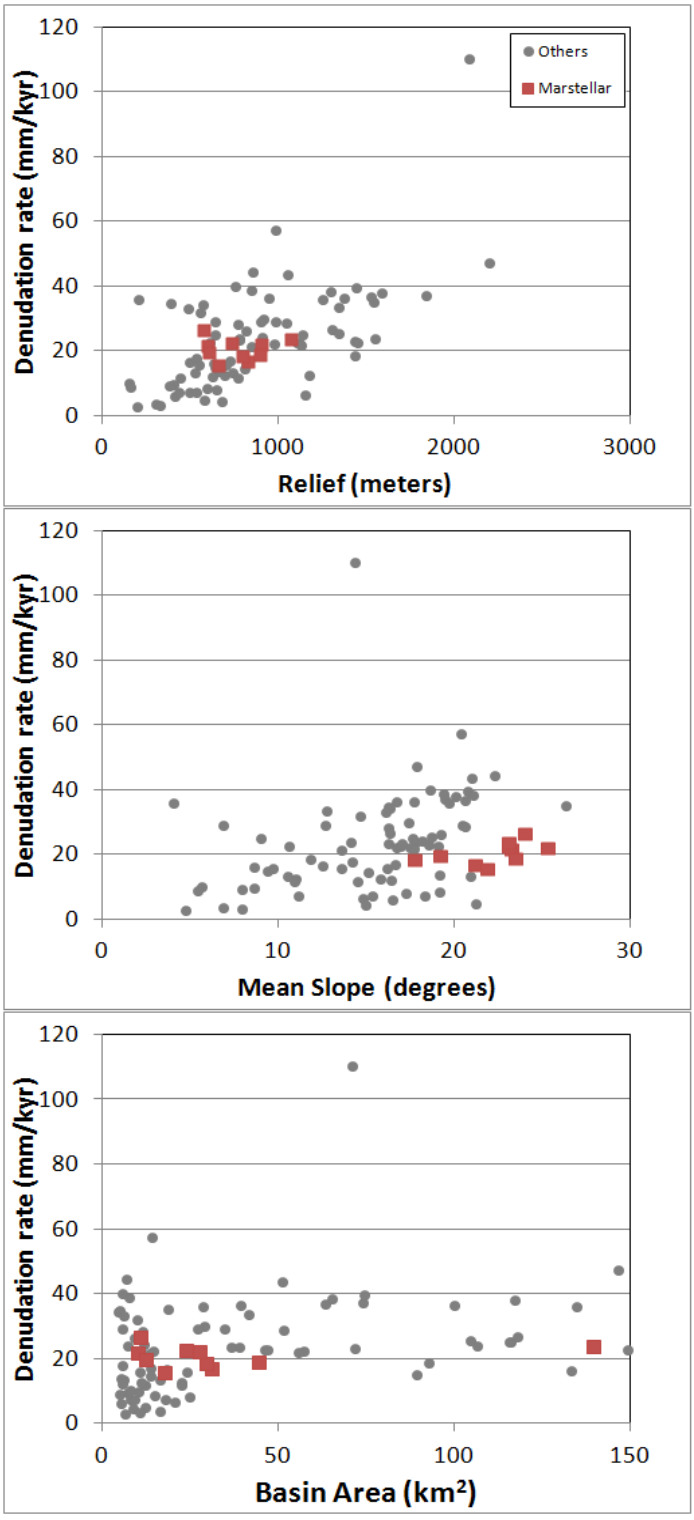

Figure 8. Comparison of Denudation rates with locations in Tectonically Inactive, Temperate Climate Zones. Basin metrics versus denudation rates with an additional 82 data points from tectonically inactive areas in temperate climate zone, similar to the southern Appalachians (Portenga and Bierman, 2011). Relief (a), mean slope (b), and basin area (c) are shown. See text for additional descriptions.

values indicate no correlation between these metrics and denudation rates in this sample set (0.1248, 0.0535, and 0.0069 for relief, slope and basin area respectively).

Figure 9 shows a comparison of our 10 basins with 84 basins from the Appalachian Mountains (Portenga and Biermann, 2011). The sample locations from the database include basins in eastern Pennsylvania, northern Virginia, western North Carolina, and the Great Smokey Mountains in Tennessee. The mean slope values for our study basins are on the higher end of the spectrum (Figure 7b), which is likely related to the fact that many of our basins comprise a portion of the Appalachian drainage divide.

Figure 9 shows that our denudation rates are fairly consistent with others from throughout the Appalachian Mountains. R^2 values indicate little to no correlation between basin morphometrics and denudation rates for the 84 comparison basins extracted from the database (0.2568, 0.2452, and 0.0538 for relief, slope and basin area, respectively).

The results shown in figures 8 and 9 are consistent with other research suggesting that tectonically inactive denudation rates show little correlation to hillslope gradient or relief (von Blankenburg 2006).

Faster denudation rates in tectonically active areas are likely driven by knickpoint migration initiated by base-level changes. The absence of significant knickpoints in our basins (Figure 5) confirms this. The ancient Appalachian Mountains are eroding at a significantly slower pace than tectonically active areas.

Our results confirm Hack's (1960) "dynamic equilibrium", which suggested that a landscape will adjust its form to attain relatively uniform erosion and retain its overall character as long as the processes operating on it remain constant.

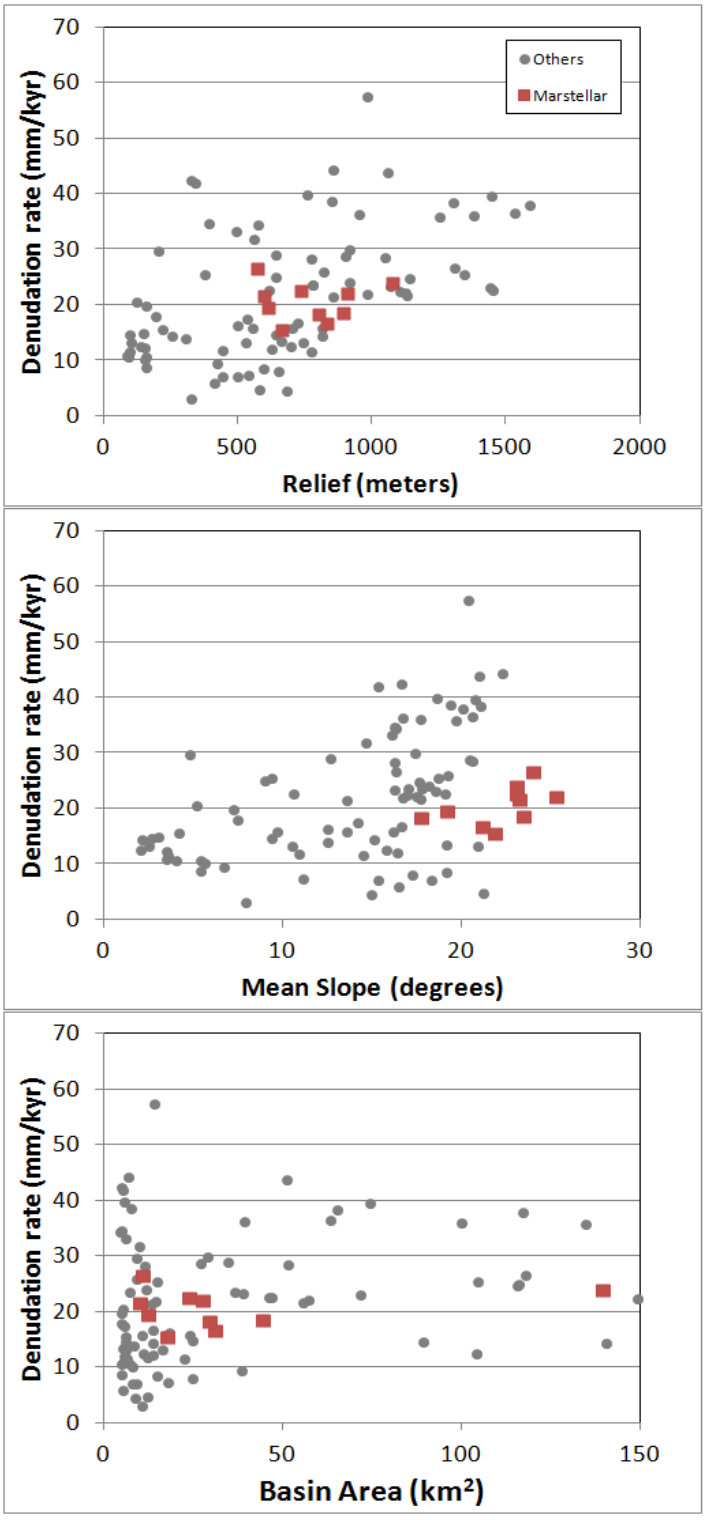

Figure 9. Comparison of Denudation rates with other Appalachian Mountain Samples. Basin metrics versus denudation rates with an additional 84 data points from the Appalachian Mountains (Portenga and Bierman, 2011). Relief (a), mean slope (b), and basin area (c) are shown. See text for additional descriptions.

CHAPTER 6

CONCLUSIONS

Our analysis provided erosion rates of 15 to 26 mm Ky^{-1} for the 0.025 to 0.050 cm sand samples and 12 to 20 mm Ky^{-1} for 3 to 8 cm gravel samples. These rates correspond well with previous studies in the Appalachian Mountains and other tectonically inactive areas. Our results are systematically lower than rates from tectonically active regions suggesting that uplift is a dominant driver of denudation rates.

We found no correlations, among our 10 study basins or a much broader database of basins from around the world, between denudation rates and relief, mean hillslope gradient, elongation, basin area or volume to area ratio. However, we found strong correlations among our ten study basins between denudation rates and hypsometric integrals. This suggests that basins with higher hypsometric integrals, and therefore more mass at higher elevations exhibit higher denudation rates as compared to lower hypsometric integrals, indicating less mass at higher elevations.

The removal of one outlier (Sample BR-0210-02 from basin 1 with a denudation rate of 12.91 ± 0.39 mm Ky^{-1}) provided strong correlations between our gravel size denudation rates and the basin metrics. This suggests that for basins fitting within an elongation range (or for basins of a certain shape), we may be able to estimate denudation rates based on various basin metrics.

While grain size analysis provided minimal numerical differences in denudation rates, we found consistent trends when comparing our gravel size grains to our basin metrics. This suggests larger grain sizes may hold greater information related to a basin's

landscape history and averaging results from multiple grain sizes may provide an even greater understanding of the watershed processes.

A larger sample size and a sampling campaign more focused on differences in geomorphic processes among basins with different hypsometry would provide us with greater confidence in the links between hypsometry, elongation and denudation rates as well as the effects of grain size sorting on watershed erosion and sediment transport processes.

Our results provide evidence that most surficial basin metrics are not good predictors of denudation rates at a global scale, but can provide some information at a regional level.

This finding supports Hack's (1960) dynamic equilibrium hypothesis of landscape evolution and casts doubt on the possibility to estimate basin-wide denudation rates and watershed sediment supply on a global scale from simple metrics of basin morphology.

APPENDIX A

CALCULATING PRODUCTION RATES FOR BASIN-WIDE DENUDATION RATES

NOTE: This document is a modification of Balco, 2001 found at http://depts.washington.edu/cosmolab/P_by_GIS.html and includes some reference to matlab files that can be found here: http://hess.ess.washington.edu/math/al_be_v22/functionlist.html

After collecting your samples and processing in the lab, you will get results in $^{10}Be/^{9}Be$ ratios. Using those ratios and Balco's 2006 paper titled "Converting Al and Be isotope ratio measurements to nuclide concentrations in quartz" you should arrive at a concentration of Number of atoms (N_{10}) and the corresponding error (error N_{10}) for each of your samples.

1. Get a DEM. You can download DEM data from seamless.usgs.gov. Download the area where your samples were collected. Name this file *demname*_grd.

Note: We recommend 1 arc second. Smaller resolution will result in much more time to calculate the items below. But smaller resolution might be needed for other processes you are doing with your data at other times. If the data is in more than one file, you need to merge them into one file using the "mosaic to new raster" tool in the data management toolbox. If the following processes become too time consuming, you can resize your DEM raster file using the "resample" tool. The DEM data should be in the following coordinate system:

> Projected coordinate system name: NAD_1983_UTM_Zone_*name*
> Geographic coordinate system name: GCS_North_American_1983

You can find your UTM zone on the internet very easily by searching for "utm zones".

You can verify your coordinate system in arc catalog under metadata on the spatial tab. If it isn't in this coordinate system, you need to project it into this coordinate system before going onto step 2. Use the "project raster" tool from the toolbox to do so.

From this DEM, you will extract your drainage basin as follows in step 2.

2. Extracting your drainage basin raster file:

a. In arcmap find "fill" and then create "fill*demname*" on raster file

b. in arcmap find "flow direction" and run on "filld*emname*" to create "*demname*_fd"

c. In arcmap, find "flow accumulation" and run it on "*demname*_fd" to create "*demname*_acc"

d. Open Arc and type:

```
Arc: &station 9999
Arc: workspace c:\workspace (The location of your DEM files)
Arc: grid
Grid: mape demname_acc
Grid: image demname_acc
```

Now zoom into basin wanted, this might take several steps to get to the exact location based on your identification of the point where your sample was collected. You might need to retype the last line to see the image as you zoom.

```
Grid: basinname_ws = watershed (demname_fd, selectpoint (filldemname, *))
```

Click on channel based on the point your sample was collected from and hit "9"

```
Grid: basinname_clip = girdpoly (basinname_ws)
Grid: arc latticeclip filldemname basinname_clip basinname_grd
```

This will leave you with files *basinname*_ws, *basinname*_clip, *basinname*_grd. (It is recommended that you kill this *basinname*_ws because you will create a new one later that is slightly different. But we recommend saving the *basinname*_clip file as it will be helpful for creating maps.)

The *basinname*_grd is the raster file we now want to work with. Your *basinname*_grd file should also be in the coordinate systems listed in step #1. (Check it now!)

3. Calculating Production Rates

A. Creating files. We now need to create several files for upload to matlab. First we need to calculate flow direction and flow accumulation on your specific basins using your *basinname*_grd file. You can do this by entering the following commands:

In Arc:

```
&station 9999
workspace c:\workspace
```

In grid:

```
basinname_fd = flowdirection(basinname_grd)
basinname_acc = flowaccumulation(basinname_fd)
basinname_cov = gridpoint(basinname_acc)
q
```

Back in arc:

```
Pointgrid basinname_cov basinname_pnt #
(note the Number is basin number and will need to be modified for each item. And then
modified later in the matlab script tlcshield.m)
Cell Size (square cell): 50
(This is the size of your DEM,  mine was 50m)
Convert the Entire Coverage(Y/N)?: y
Enter background value (NODATA | ZERO): nodata
grid
```

Back in grid:

```
Basinname_ws = watershed(demname_fd,basinname_pnt)
```

You now have a grid called *basinname*_ws in which defines pixels we are interested in. We can now kill other files.

In grid:

```
kill basinname_fd
kill basinname_acc
kill basinname_cov
kill basinname_pnt
```

B. Latitudes. Now you need a grid containing the latitudes of all the pixels. Since USGS 30-meter DEM's are in UTM coordinates, this is a fairly elaborate sequence of GRID commands:

If not aready in arc:

```
&station 9999
workspace c:\workspace
grid
```

In grid:

```
/* extract relevant elevations

basinname_elv = con( ^ isnull(basinname_ws),demname_grd)

/* reproject to geographic

basinname_elvg = project(^ isnull(basinname_elv))
output
projection geographic
units dd
datum nad27
parameters
end

/* dump latitudes

&describe basinname_elvg
setcell basinname_elvg
setwindow basinname_elvg
basinname_lat = (%grd$ymax% - (%grd$dy% / 2)) - (( $$rowmap - 1 ) * %grd$dy% )

/* reproject back into UTM
/* make sure to change UTM zone as needed

basinname_utm = project(basinname_lat)
input
projection geographic
units dd
parameters
output
projection utm
zone 17
units meters
parameters
end

/* clip
setwindow basinname_elv
setcell basinname_elv
latbasinname = con( ^ isnull(basinname_elv),basinname_utm)
```

```
/* partial cleanup

kill basinname_elvg
kill basinname_lat
kill basinname_elv
kill basinname_utm
```

Now we have a grid called "latbasinname" which contains latitudes for all the pixels in the watersheds we want to analyze.

Next we need grids containing the x and y coordinates of each pixel. In GRID, issue:

```
&describe basinname_ws
setcell basinname_ws
setwindow basinname_ws
ygrid# = (%grd$ymax% - (%grd$dy% / 2)) - ( $$rowmap * %grd$dy% )
xgrid# = (%grd$xmin% + (%grd$dx% / 2)) + ( $$colmap * %grd$dx% )
```

Note: type these exactly, include spaces, or you'll get an error message.

One more grid is also required. Most pixels in the image are not on ridgelines and will not significantly contribute to topographic shielding of most other points. In the shielding calculation for each pixel we consider two groups of other pixels in the landscape: one, pixels near the pixel of interest, and two, pixels on ridgelines. We ignore all the other pixels. This greatly reduces execution time. The "ridgeline" pixels are most easily obtained by taking only those pixels which have a flow accumulation value of zero:

In grid:

```
screen = con((demname_acc EQ 0),1,0)
```

It's easiest to get ARC grids into MATLAB by exporting ASCII files:

```
elv.txt = gridascii(int(demname_grd))
wsheds.txt = gridascii(basinname_ws)
lat.txt = gridascii(latbasinname)
xgrid.txt = gridascii(int(xgrid#))
ygrid.txt = gridascii(int(ygrid#))
screen.txt = gridascii(screen)
```

Then use notepad to remove the first six lines of each text file. (This is header information included by ARC that we don't need.)

C. Latitude/altitude correction. You will use MATLAB to do the latitude/altitude correction. (I created a script called lat_alt.m)

In MATLAB, load these grids:

```
load elv.txt -ascii
load wsheds.txt -ascii
load lat.txt –ascii
load xgrid.txt –ascii
load ygrid.txt -ascii
load screen.txt –ascii
```

Then use the m-file stone2000.m to do the latitude/altitude correction. You will also need the m-file stdatm.m . (These files should already be saved in your matlab current folder).

To do this, issue the following in MATLAB:

```
t_elv = reshape(elv,size(elv,1)*size(elv,2),1);
t_lat = reshape(lat,size(lat,1)*size(lat,2),1);
tt_elv = elv(find(lat ~= -9999));
tt_lat = lat(find(lat ~= -9999));
tt_p = stdatm(tt_elv);
tt_corr = stone2000(tt_lat,tt_p);
lacorr = zeros(size(elv));
lacorr(find(lat~=-9999)) = tt_corr;
```

Now lacorr is a MATLAB variable containing the latitude/altitude correction factor for each pixel of interest. It should look like this:

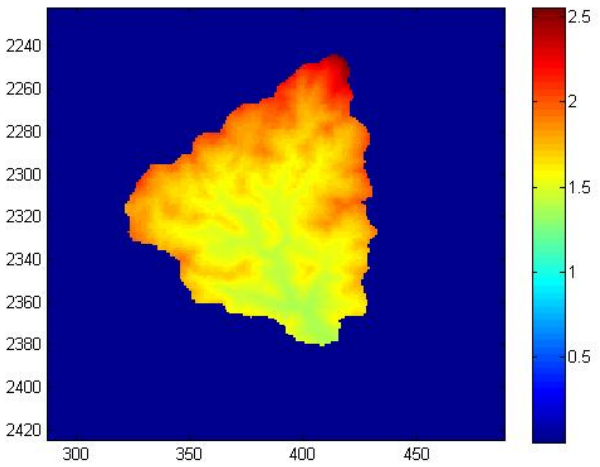

D. Topographic shielding. Next, we need to calculate the topographic shielding for all the pixels we are interested in. (If you just care about one pixel it can be done in ARC/INFO using an AML script called point_s.aml.)

If you care about all the pixels in a watershed, it is faster to do this in MATLAB. Keep in mind that this is a very time-consuming operation and may require many hours of machine time for a watershed of even moderate size.

In matlab you can use tlmshield.m to calculate topographic shielding for each pixel. This is a modified version of shielding.m by Balco found on the cronus website. In the first line you will need to define your watershed number per the number you used above in step 3A.

This results in a matrix called shield# that contains shielding factors for each pixel of interest.

Here is an example:

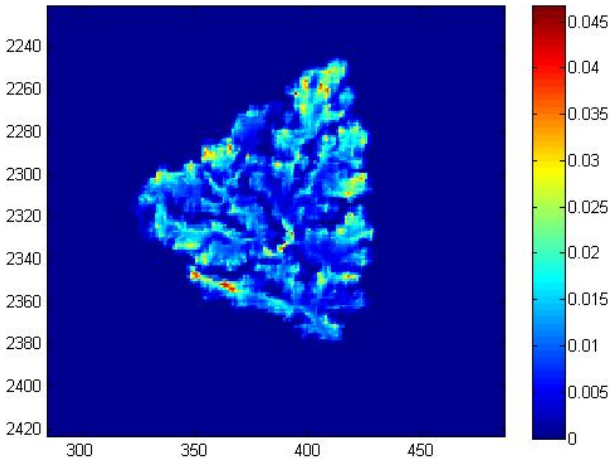

E. Total isotope production rate. The last thing to do is assemble all this into a grid showing production rate in all pixels. (I've created a script called prod_rate.m for these steps.)

Load the shielding and lat/alt correction matrices into MATLAB and do:

```
totalcorr = lacorr .* (1 - s_factor);
p = 4.49; % Stone et al production rate: can be modified.
p_all = totalcorr.*p;
```

Then average the values for p_all in the watershed. Here is an example of what that should look like.

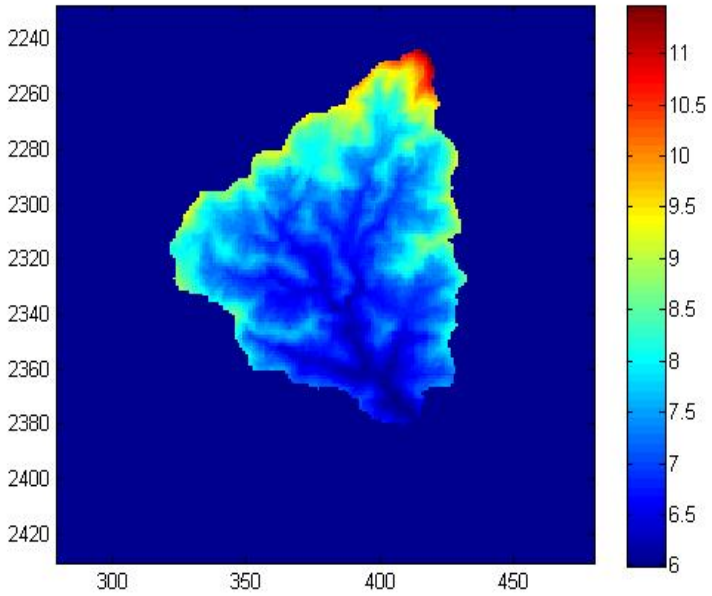

Instead of using the prod_rate.m file to calculate production rates, we used totcorr.m to calculate scaling factors and then used those scaling factors and the Cosmocalc excel addin (Vermeesh, 2007), to get erosion rates based on 5 different production rates provided within cosmocalc.

APPENDIX B

CALCULATING BASIN METRICS USING ARCGIS PROGRAMS

Note: If you've already calculated your production rates using "Calculating Production Rates for Basin-wide Denudation Rates" some of these steps may have already been done. But they may have been done using a different resolution. For this process you want a smaller resolution so you may want to start over with your DEM file from scratch if you resized your DEM file during the production rate calculations. If you didn't change your resolution, then you can use the files previously created.

1. Get a DEM. You can download DEM data from seamless.usgs.gov. Download the area where your samples were collected. Name this file *demname*_grd.

Note: We recommend 1/3 arc second (~10 meter DEM). You may have used a larger resolution for your production rate calculations, but use the smaller resolution now.

If the data is in more than one file, you need to merge them into one file using the "mosaic to new raster" tool in the data management toolbox.

If any of the following processes become too time consuming, you can resize your DEM raster file using the "resample" tool. The DEM data should be in the following coordinate system:

> Projected coordinate system name: NAD_1983_UTM_Zone_*name*
> Geographic coordinate system name: GCS_North_American_1983

You can find your UTM zone on the internet very easily by searching for "utm zones".

You can verify your coordinate system in arc catalog under metadata on the spatial tab. If it isn't in this coordinate system, you need to project it into this coordinate system before going onto step 2. Use the "project raster" tool from the toolbox to do so.

From this DEM, you will extract your drainage basin as follows in step 2.

2. Extracting your drainage basin raster file:

a. In arcmap find "fill" and then create "fill*demname*" on raster file

b. in arcmap find "flow direction" and run on "filld*emname*" to create "*demname*_fd"

c. In arcmap, find "flow accumulation" and run it on "*demname*_fd" to create "*demname*_acc"

d. Open Arc and type:

```
Arc: &station 9999
Arc: workspace c:\workspace (The location of your DEM files)
Arc: grid
Grid: mape demname_acc
Grid: image demname_acc
```

Now zoom into basin wanted, this might take several steps to get to the exact location based on your identification of the point where your sample was collected. You might need to retype the last line to see the image as you zoom.

```
Grid: basinname_ws = watershed (demname_fd, selectpoint (filldemname, *))
```

Click on channel based on the point your samples was collected from and hit "9"

```
Grid: basinname_clip = girdpoly (basinname_ws)
Grid: arc latticeclip filldemname basinname_clip basinname_grd
```

This will leave you with files *basinname*_ws, *basinname*_clip, *basinname*_grd. The *basinname*_grd is the raster file we now want to work with. Your *basinname*_grd file should also be in the coordinate systems listed in step #1. (Check it now!)

Basin Metrics

A. Basin Relief

This will provide you with Minimum Values, Maximum Value. The difference between these two values is the relief for your drainage basin.

In Arc:

```
Arc: describe basinname_grd
```

B. Basin Slope

This will provide you with a Minimum Value (usually zero), Maximum Value, and Mean. These are your slopes in degrees.

In Arc:

```
Arc: grid
Grid: basinname_slp = slope (basinname_grd, degree)
Grid: describe basinname_slp
```

C. Basin Hypsometry

Drainage basin hypsometry describes the distribution of elevation across an area of land. A useful attribute of the hypsometric curve is that drainage basins of different sizes can be compared with each other because area and elevation are plotted as functions of total area and total elevation. A high hypsometric integral indicates a "youthful" landscape and vice versa.

In Grid:

```
Grid: b#_slice = slice (basinname_grd, eqinterval, 10)
Grid q
Arc: info
ENTER USER NAME> arc
ENTER COMMAND >select B#_SLICE.VAT          Note: Case sensitive!! Use all uppercase!
ENTER COMMAND >export c:\workspace\b#_slice.dat sdf
ENTER COMMAND > q stop
```

This b#_slice.dat file will give you information needed to create hypsometric graphs in two columns. Column one is the number of elevation buckets. Column two is the number of cells in each of those buckets. You want to graph elevation/total elevation on the Y-axis and area/total area of each bucket on the X-axis.

To calculate your hypsometric integral use:

$$HI = \frac{mean\ elevation - maximum\ elevation}{maximum\ elevation - minimum\ elevation}$$

D. Drainage basin elongation

Basin elongation is defined as the maximum length divided by the maximum width. In ArcMap, use the "Measure distance and area" tool to find the maximum length and maximum with of your drainage basin. Measure the length along the most prominent stream.

E. Drainage Basin Volume to Area Ratio

Basin Volume to Area Ratio is a metric that indicates the degree of dissection in a landscape. The volume of rock eroded is normalized to the basin area and, like hypsometry, it is useful when comparing basins of different sizes.

We want to work with two different sizes of DEMs. Beginning with your highest resolution DEM, determine the approximate data size in meters. A 1 arcsecond DEM is approximately 30 m and a 1/3 arcsecond DEM is approximately 10 m. Note: these are not precise.

Start with the DEM for each basin that has the highest resolution. For example, we have a 1/3 arc second DEM for each basin. So we are beginning with DEMs of approximately 10 m. Using this higher resolution DEM, we will create our second lower resolution (larger size) DEM.

We're going to resample my ~10 m DEM to both an exact 10 m DEM and a 30 m DEM. This can be done using the "resample" tool in arcmap or arc catalogue or in Grid.

In grid:

Grid: *bname*10_grd = resample (*basinname*_grd, 10, bilinear)
Grid: *bname*30_grd = resample (*bname*10_grd, 30, bilinear)

We now have a 10m and 30m DEM to work with. Now we need to create a maximum elevation envelope map for the resampled data.

Grid: *bname30*_#mx = focalmax (*bname*30_grd, circle, #)

The number in the focalmax command describes the radius (in number of cells, so this measured length varies depending on your resolution) of the low pas circular filter being

used on the topography and can be changed depending on how "tightly" you want to stretch the maximum elevation envelope map over the topography.

I used 1, 5, 10, 25, and 50 for comparisons. (100 was initially tried, but was too large for some of the basins.)

Now we need to resample our 30m maximum elevation map back down to 10m so our 10m DEM topography can be subtracted from it.

```
Grid: bname10_#mx = resample (bname30_#mx, 10, bilinear)
Grid: bname#_res = bname10_#mx – bname10_grd
Grid: q
Arc: latticetin bname#_res bname#_tin
Arc: volume bname#_tin
```

The volume and area will be reported. Divide the volume by the area and record the value.

E. Long profile

First, consider how much information you want from your long profile. You'll want to use either your basinname_acc file or you might want to consider using a new DEM to capture your stream downstream from your collection site. We had several basins that flowed into the same larger stream so we went back out to gather a DEM that wasn't as large as my initial DEM, but bigger than my basin DEM. You can clip a larger DEM you already have, if your location doesn't provide easy access to a new DEM online.

Using the appropriate flow accumulation file (if you have a new file, go through the steps in 1, 2a, b, & c to get your file ready for these steps).

In grid:

```
Grid: b#_stm = con (demname_acc > 100, 1)
Grid: mape b#_stm
Grid: image b#_stm
```

The number 100 means that any cell with more than 100 cells flowing into it will be a stream, all other cells are hillslopes. If after looking at your stream file, you find too

many streams, you can adjust it upward as long as you continue to have complete streams. (I used 1000).

```
Grid: b#_cov = gridline (b#_stm)
```

It is recommended that you make a copy of your b#_cov file before you start editing, to do so:

```
Grid: copy b#_cov  b#copy_cov
Grid: q
```

You can now start editing:

```
Arc: arcedit
Arcedit: mape b#_cov
Arcedit: edit b#_cov
Arcedit: de all
Arcedit: ef arc
Arcedit: draw
Arcedit: select many
```

Arcedit will now allow you to select all the streams you do not want. Using arcmap to look at both your flow accumulation file and your b#_cov file select the items you do not want. Those items will turn yellow. When you are ready to delete, hit 9.

```
Arcedit: delete
```

It is recommended that you save routinely. If you accidentally select something you don't want to delete, just type in "select many" again and start again. You can also do "select circle" to remove large areas at once.

```
Arcedit: save
```

When you are completely done and have a line representing your trunk channel.

```
Arcedit: select all
Arcedit: unsplit
Arcedit: save
Arcedit: q
```

You now need to extract the elevations that correspond with the trunk channel.

```
Arc:  grid
Grid: mape filldemname
```

```
Grid: image filldemname
Grid: setcell filldemname
Grid: s#_grd = linegrid (b#_cov)
Grid: setmask s#_grd
Grid: lp#_grd = filldemname
Grid: setmask off
Grid: lp#_int = int(lp#_grd)
Grid: q
```

The elevation data now resides in a file called lp#_int.vat. We now want to export this file.

```
Arc:  info
ENTER USER NAME>  arc
ENTER COMMAND>  select LP#_INT.VAT
ENTER COMMAND> export /yourfilefoldername/lp#.dat sdf
ENTER COMMAND> q stop
```

If you now go to your file folder and open the lp#.dat file, you will find two columns. The first column is the elevations. The second column is the number of points of that particular elevation. The distance between the adjacent elevations is determined by your DEM cell size. Using this file you can make a plot of distance versus elevation.

APPENDIX C

COSMOGENIC NUCLIDE SAMPLE SITE IMAGES

Basin 1

Basin 2

Basin 3

Basin 4

Basin 5

Basin 6

Basin 7

Basin 8

Basin 9

Basin 10

REFERENCES

Ahnert, F., 1970. Functional relationships between dunudation, relief and uplift in large mid-latitude drainage basins. American Journal of Science, 268, 243-263.

Balco, G., et al., 2008. A complete and easily accessible means of calculating surface exposure ages or erosion rates from ^{10}Be and ^{26}Al measurements. Quaternary Geochronology, v. 3, p. 174-195.

Belmont, P., et al., 2007. Cosmogenic 10Be as a tracer for hillslope and channel sediment dynamics in the Clearwater River, western Washington State. Earth & Planetary Science Letters, 264, 123-135.

Bierman, P.R., et al., 2002. Rates and timing of earth surface processes from in-situ-produced cosmogenic Be-10, in Grew, E.S., ed., Beryllium. Mineralogy, Petrology, and Geochemistry, Reviews in Mineralogy and Geochemistry, 50, 148-205.

Bierman, P.R., and Nichols, K.K., 2004. Rock to sediment-slope to sea with ^{10}Be-rates of landscape change. Ann. Rev. Earth Planetary Science Letters. 32, 215-255.

Binnie, S., et al., 2006. Sediment mixing and basin-wide cosmogenic nuclide analysis in rapidly-eroding mountainous environments. Quat.Geochem. 1, 4–14.

Brocklehurst, S. H. and Whipple, K. X., 2004, Hypsometry of glaciated landscapes. Earth Surface Processes and Landforms, 29: 907–926. doi: 10.1002/esp.1083

Brown, E., et al., 1995. Denudation rates determined from the accumulation of in situ-produced ^{10}Be in the Luquillo Experimental Forest, Puerto Rico: Earth and Planetary Science Letters, 129, 193-202.

Davis, W.M., 1889. The rivers and valleys of Pennsylvania. National Geographic Magazine, 1, 183-253.

Densmore, A.L., et al., 2009. Spatial variations in catchment-averaged denudation rates from normal fault footwalls. Geology, 37, 1139-1142.

Desilets, D., and Zreda, M., 2003. Spatial and temporal distribution of secondary cosmic-ray nucleon intensities and applications to in-situ cosmogenic dating. Earth and Planetary Science Letters, 206, 21–42.

Desilets, D., et al., 2006. Extended scaling factors for in situ cosmogenic nuclides. New measurements at low latitude. Earth and Planetary Science Letters, 246, 265–276.

Dicken, C.L., et al., 2005. Preliminary integrated geologic map databases for the United States: Alabama, Florida, Georgia, Mississippi, North Carolina, and South Carolina: USGS, Open-File Report OF-2005-1323, scale 1:500000.

Dunai, T., 2010. Cosmogenic Nuclides: Principles, Concepts, and Applications in the Earth Surface Sciences. Cambridge University Press, Cambridge, UK.

Eaton, L.S., et al., 2003. Role of debris flows in long-term landscape denudation in the central Appalachians of Virginia. Geology, 31, 339-342.

Gallen, S. F., et al., 2011. Hillslope response to knickpoint migration in the Southern Appalachians: implications for the evolution of post-orogenic landscapes. Earth Surface Processes and Landforms, 36: 1254–1267. doi: 10.1002/esp.2150

Gosse, J.C. and Phillips, F.M., 2001. Terrestrial in situ cosmogenic nuclides: theory and application. Quat. Sci. Rev. 20, 1470-1560.

Granger, D., et al, 1996. Spatially averaged long-term erosion rates measured from in situ-produced cosmogenic nuclides in alluvial sediment. Journal of Geology, 104, 249.

Hack, J.T., 1960. Interpretation of erosional topography in humid temperate regions. American Journal of Science, 258, 80-97.

Hancock, G. and Kirwan, M., 2007. Summit erosion rates deduced from 10Be: Implications for relief production in the central Appalachians. Geology, 35, 89.

Hatcher, R.D., 2010. From Rodina to Pangea; the lithotectonic record of the Appalachian Region. Geological Society of America Memoir, 206, 1-19.

Heimsath, A.M., et al., 2001. Late Quaternary erosion in southeastern Australia: a field example using cosmogenic nuclides. Quarternary International, 83-5, 169-185

Judson, S. and Ritter, D.F., 1964.Rates of regional denudation in the United States. Journal of Geophysical Research, 69, 3395-3401.

Lal, D., 1991. Cosmic ray labeling of erosion surfaces: In situ nuclide production rates and erosion models. Earth and Planetary Science Letters, 104, 424-439.

Matmon, A., et al., 2003.Erosion of an ancient mountan range, the Great Smokey Mountains, North Carolina and Tennessee. American Journal of Science, 303, 972-973.

Niemi, N.A., et al., 2005. Effects of bedrock landslides on cosmogenically determined erosion rates. Earth and Planetary Science Letters, 237, 480–498.

Pazzaglia, F. J., 2003, Landscape evolution models, in Gillespie, A. R., Porter, S. C., and Atwater, B. F., eds., The Quaternary Period in the United States: Amsterdam, Elsevier, p. 247-274, doi:10.1016/S1571-0866(03)01012-1

Pazzaglia, F. J., and Gardner, T. W., 2000. Late Cenozoic landscape evolution of the US Atlantic passive margin: insights into a North American Great Escarpment, in Summerfield, M. A., editor, Geomorphology and Global Tectonics: Chichester, John Wiley, p. 283-303.

Poag, C.W. and Sevon, W.D., 1989. a record of Appalachian denudation in postrift Mesozoic and Cenozoic sedimentary deposits of the U.S. middle Atlantic continental margin. Geomorphology, 2, 119-157.

Portenga, E. and Bierman, P. R., 2011. Understanding Earth's Eroding Surface with ^{10}Be. GSA Today.

Pratt-Sitaula, B., et al., 2004. Landscape disequilibrium on 1000–10,000 year scales Marsyandi River, Nepal, central Himalaya. Geomorphology, 58, 223.

Roering, J.J., et al., 2007. Functional relationships between denudation and hillslope form and relief. Earth and Planetary Science Letters, 264, 245-258.

Slingerland, R. and Furlong. K.P., 1989. Geodynamic and geomorphic evolution of the Permo-Triassic Appalachian mountains, Geomorphology, 2, 23-27.

Southern Appalachian Man and the Biosphere. 1996. The Southern Appalachian Assessment Social/Cultural/Economic Technical Report (Report 4 of 5). Atlanta: USDA Forest Service, Southern Region. 219 p.

Spotila et al., 2004, Origin of the Blue Ridge escarpment along the passive margin of Eastern North America. Basin Reserach, v. 16, p. 41-63.

Stock, G.M., et al., 2009. Spatial and temporal variations in denudation of the Wasatch Mountains, Utah, USA: Lithosphere, v. 1, p. 34-40, doi:10.1130/L15.1.

Strahler, A.N., 1952. Hypsometric (area-altitude) analysis of erosional topography. Bulletin of the Geological Society of America, 63, 1117-1142.

Stone, J.O., 2000, Air pressure and cosmogenic isotope production. Journal of Geophysical Research, 105, 23,753-23,759.

Thomas. W.A., 2006. Tectonic inheritance at a continental margin. GSA Today, 16(2), 4-11.

Vermeesch, P., 2007. CosmoCalc: an Excel add-in for cosmogenic nuclide calculations. Geochemistry Geophysics Geosystems. 8, Q08003.

von Blanckenburg, F., 2006. The control mechanisms of erosion and weathering at basin scale from cosmogenic nuclides in river sediment, Earth and Planetary Science Letters, 237, 3-4, 462-479.

Willenbring, J.K., and von Blanckenburg, F., 2010. Meteoric cosmogenic Beryllium-10 adsorbed to river sediment and soil: Application for Earth-surface dynamics. Earth-Science Reviews, 98, 105-122.

Wobus, C., et al., 2005. Active out-of-sequence thrust faulting in the central Nepalese Himalaya. Nature, 434, 1008-1011.

Yanites, B., et al., 2009. Numerical and Analytical Models of Cosmogenic Radionuclide Dynamics in Landslide-dominated Drainage Basins. Journal of Geophysical Research 114. F01007.